Studies on the Therapeutic Potential of Phosphodiesterase 10A-Specific Inhibition for Huntington's Disease

January 2018

Akina HARADA

Studies on the Therapeutic Potential of Phosphodiesterase 10A-Specific Inhibition for Huntington's Disease

A Dissertation Submitted to

the Graduate School of Life and Environmental Sciences,

the University of Tsukuba

in Partial Fulfillment of the Requirements

for the Degree of Doctor of Philosophy in Biological Science

(Doctoral Program in Biological Sciences)

Akina HARADA

Table of Contents

Abstract

Huntington’s disease (HD) is an inherited neurodegenerative disorder characterized by progressive loss of striatal medium spiny neurons (MSNs) that constitute direct and indirect pathways. Impairment of cAMP and cGMP signaling is hypothesized as one of the molecular mechanisms underlying degeneration of MSNs. Phosphodiesterase 10A (PDE10A) degrades both cAMP and cGMP, and is selectively expressed in both direct and indirect pathway MSNs. Therefore, PDE10A inhibition is considered to be a promising strategy for the treatment of HD symptoms. In HD, indirect pathway MSNs are more vulnerable to degeneration than direct pathway MSNs, thus a balanced activation of both MSNs, which means a biased activation of indirect pathway MSNs, is likely to be more beneficial for patients with HD.

To test this hypothesis, I obtained Cmpd-A, a tool compound which specifically inhibits PDE10A *in vivo*, and induces the balanced activation of both MSNs. Cmpd-A potently and selectively inhibited human recombinant PDE10A *in vitro*. Autoradiography studies using rat brain slices indicated that Cmpd-A binds to native PDE10A with high binding affinity. *In vivo* autoradiography and PDE10A occupancy studies revealed that Cmpd-A can readily penetrate into the brain and selectively bind to native PDE10A in living rats. In addition, a previous study showed that Cmpd-A induced the biased activation of indirect pathway MSNs in rats.

In the R6/2 mouse model of HD, repeated treatment with Cmpd-A suppressed the reduction of BDNF levels, prevented striatal neurodegeneration, and suppressed the increase in seizure frequency. As for motor deficits, Cmpd-A suppressed the development of clasping behavior

and decreased locomotor activity in the open field in R6/2 mice. Regarding cognitive function, Cmpd-A improved deficits in procedural learning in R6/2 mice.

These results suggest that the balanced activation of both direct and indirect pathway MSNs based on specific and unique PDE10A inhibition has a potential to improve HD symptoms. Moreover, the findings in the current study will help us better understand the biological function of PDE10A.

Abbreviations

ARG, autoradiography

BDNF, brain-derived neurotrophic factor

Bs, brain stem

CAG, cytosine-adenine-guanine

cAMP, cyclic adenosine monophosphate

Cb, cerebellum

cGMP, cyclic guanosine monophosphate

CFC, contextual fear conditioning

CNS, central nervous system

CPu, caudate putamen

CREB, cAMP response element-binding protein

EPS, extrapyramidal symptoms

Fcx, frontal cortex

GP, globus pallidus

HD, Huntington's disease

HE, hematoxylin and eosin

hPDE10A, human recombinant PDE10A

IC_{50} value, half-maximal inhibitory concentration

KO, knockout

mHTT, mutant huntingtin

MS, mass spectrometry

MSNs, medium spiny neurons

NAc, nucleus accumbens

NORT, novel object recognition test

NSB, non-specific binding

PBS, phosphate buffered saline

PDE, phosphodiesterase

PSL, photostimulated luminescence

RM-ANOVA, repeated measures analysis of variance

ROI, region of interest

RT, room temperature

SD, Sprague-Dawley

SN, substantia nigra

Str, striatum

Tg, transgenic

Thal, thalamus

TBZ, tetrabenazine

WT, wild-type

General Introduction

Huntington's disease (HD) is an autosomal dominant inherited, progressive neurodegenerative disorder with a variable phenotype including motor dysfunction such as chorea and dystonia, cognitive impairment, and psychiatric disturbances such as significant changes in personality or mood (Ross and Tabrizi, 2011; Scheuing *et al.*, 2014; Walker, 2007). The prevalence of HD is roughly 6 cases per 100,000 people in the western nations including North America, Europe, and Australia, and the typical latency from onset to death is 15-20 years (Ross and Tabrizi, 2011; Scheuing *et al.*, 2014; Walker, 2007). These severe symptoms of HD seriously debilitate the quality of life not only in patients but also in their families and caregivers. HD is caused by a pathogenic cytosine-adenine-guanine (CAG) trinucleotide repeat expansion (more than 35 repeats) at exon 1 of the *huntingtin* gene, which encodes the mutant huntingtin protein (mHTT) including an expanded polyglutamine tract, resulting in the toxic aggregate formation of mHTT (Ross and Tabrizi, 2011; Scheuing *et al.*, 2014). Despite the ubiquitous expression of HTT throughout the brain and body, prominent atrophy and cell loss occur selectively in the striatum (Ross and Tabrizi, 2011; Walker, 2007). Approximately 95% of the striatal neurons are inhibitory projection neurons termed medium spiny neurons (MSNs) (Reinius *et al.*, 2015). MSNs are known to be the most vulnerable to the degeneration in HD although the exact mechanism underlying this selective vulnerability has not yet been elucidated (Ross and Tabrizi, 2011; Scheuing *et al.*, 2014; Walker, 2007).

Tetrabenazine (TBZ) is the only Food and Drug Administration-approved drug indicated

for the treatment of chorea associated with HD (Frank, 2014). Although the efficacy of TBZ as an antichoreic drug has been clearly demonstrated in a double-blind, placebo-controlled clinical study, TBZ can cause adverse events such as akathisia, depression, dizziness, or parkinsonism (Frank, 2014). Moreover, TBZ does not halt disease progression, nor does it treat psychiatric symptoms associated with HD (Scheuing *et al.*, 2014). Because the causal gene, *mHtt*, has already been identified, several gene silencing or repairing therapies have been preclinically studied for the treatment of HD (Godinho *et al.*, 2014). So far, however, there are still some limitations to clinical application, such as the lack of effective and nontoxic strategies for the delivery of such technologies to the brain, off-target adverse effects, and the saturation of endogenous gene-silencing pathways (Godinho *et al.*, 2014). Thus, disease-modifying therapies are still of great values for patients with HD.

Intracellular cyclic adenosine and guanosine monophosphate (cAMP and cGMP) play important roles as second messenger molecules controlling multiple cellular processes. Impairment in cAMP signaling and its downstream cAMP response element-binding protein (CREB) signaling pathway by mHTT has been hypothesized to play a critical role in the neurodegeneration of HD pathology (Choi *et al.*, 2009; Gines *et al.*, 2003; Mantamadiotis *et al.*, 2002; Nucifora *et al.*, 2001; Sugars and Rubinsztein, 2003; Wyttenbach *et al.*, 2001). In addition, neuronal nitric oxide synthase mRNA is also decreased in the postmortem striatum of patients with HD (Norris *et al.*, 1996), suggesting the downregulation of cGMP signaling.

Phosphodiesterase 10A (PDE10A) is an enzyme degrading both cAMP and cGMP, and is selectively expressed in the striatum in mammals including mice, rats, monkeys, and humans (Bender and Beavo, 2006; Coskran *et al.*, 2006; Fujishige *et al.*, 1999; Seeger *et al.*, 2003). PDE10A inhibition enhances cAMP and cGMP signaling selectively in MSNs, thus it may be a promising strategy for the treatment of HD (Fig.1).

There are 11 different families of PDEs comprising 21 different gene products, and each PDE superfamily enzyme shows a distinct distribution pattern and has important functions (Bender and Beavo, 2006). Therefore, a brain permeable inhibitor specific for PDE10A under physiological condition is extremely useful as a tool to test the therapeutic potential of PDE10A inhibition for HD symptoms. In part 1, I focused on discovering a tool inhibitor specific for PDE10A. By high-throughput screening from thousands of chemical seeds and structure-based drug design using X-ray crystal structure of PDE10A catalytic domain, Cmpd-A was identified as a potent and specific inhibitor of human recombinant PDE10A (hPDE10A) *in vitro* (Kunitomo *et al.*, 2014). Binding and functional activities of compounds for recombinant proteins are potentially different from those for proteins under physiological condition due to differences in protein folding and/or binding partners. Therefore, I also checked binding activity and selectivity of Cmpd-A for naive PDE10A in rodents. *In vitro* autoradiography (ARG) study demonstrated that Cmpd-A selectively accumulates in the areas where PDE10A is highly expressed with a high binding affinity. Moreover, *in vivo* ARG study

and PDE10A occupancy study revealed that orally administered Cmpd-A readily penetrates into the rat brain and selectively binds to PDE10A *in vivo*. Thus, I obtained Cmpd-A, a brain penetrating inhibitor specific for native PDE10A under physiological condition.

The R6/2 mouse is a widely used transgenic mouse model of HD due to its robust phenotype with an early onset, rapidly progressive neurodegeneration, weight loss, and motor and cognitive deficits (Pouladi *et al.*, 2013). Thus, in part 2, I evaluated the effects of Cmpd-A on various phenotypes in R6/2 mice to predict the therapeutic potential of PDE10A-specific inhibition for HD symptoms. Brain-derived neurotrophic factor (BDNF), a putative CREB-regulated molecule, is crucial for activity and survival of MSNs (Choi *et al.*, 2009; Zuccato and Cattaneo, 2007). R6/2 mice showed reduced striatal BDNF levels, striatal atrophy, higher frequency of stress-induced seizures, and body weight loss. These mice also exhibited clasping behavior, a cardinal phenotype of HD model mice, and various motor and cognitive deficits. Repeated treatment with Cmpd-A suppressed the reduction of striatal BDNF levels, prevented striatal atrophy, and suppressed the increase in seizure frequency. Cmpd-A treatment also suppressed the development of clasping behavior and motor dysfunction in the open field test, and improved deficits in procedural learning.

These results obtained from the two studies suggest that specific inhibition of PDE10A is potentially effective for several HD symptoms (Fig. 1).

Part 1

Characterization of Binding and Inhibitory Properties of Cmpd-A, A Tool Phosphodiesterase 10A Inhibitor

Abstract

Phosphodiesterase 10A (PDE10A) inhibition is a novel and promising approach for the treatment of central nervous system disorders such as schizophrenia and Huntington's disease. A novel PDE10A inhibitor, Cmpd-A [1-[2-fluoro-4-(1*H*-pyrazol-1-yl)phenyl]-5-methoxy-3-(1-phenyl-1*H*-pyrazol-5-yl)-pyridazin-4(1*H*)-one] has shown high inhibitory activity and selectivity for human recombinant PDE10A2 *in vitro*; the half-maximal inhibitory concentration was 0.30 nM, and selectivity over other phosphodiesterases (PDEs) was more than 15000-fold. Cmpd-A at 10 μM did not show more than 50% inhibition or stimulation of 91 enzymes or receptors except for PDEs. *In vitro* autoradiography (ARG) studies using rat brain sections revealed that [^{3}H]Cmpd-A selectively accumulated in the caudate putamen (CPu), nucleus accumbens (NAc), globus pallidus, substantia nigra, and striatonigral projection, where PDE10A is highly expressed. This [^{3}H]Cmpd-A accumulation was almost entirely blocked by an excess amount of MP-10, a PDE10A selective inhibitor, and the accumulation was not observed in brain slices of *Pde10a*-knockout mice. In rat brain sections, [^{3}H]Cmpd-A bound to a single high-affinity site with mean ± SEM dissociation constants of 7.2 ± 1.2 and 2.6 ± 0.5 nM for the CPu and NAc shell, respectively. Orally administered [^{14}C]Cmpd-A selectively accumulated in PDE10A expressing brain regions in an *in vivo* ARG study in rats. Striatal PDE10A occupancy by Cmpd-A *in vivo* was measured using T-773 as a tracer and a dose of 0.88 mg/kg (p.o.) was

calculated to produce 50% occupancy in rats. Translational studies with Cmpd-A and other PDE10A inhibitors such as those presented here will help us better understand the pharmacological profile of this class of potential central nervous system drugs.

Introduction

Intracellular cAMP and cGMP play important roles as second messenger molecules controlling multiple cellular processes. Phosphodiesterases (PDEs) are enzymes that regulate cellular levels of these cyclic nucleotides by regulating their degradation rates (Bender and Beavo, 2006). There are 11 different families of PDEs comprising 21 different gene products, and each PDE superfamily enzyme shows a distinct distribution pattern and has important functions (Bender and Beavo, 2006). PDE10A **is** a **dual**-substrate PDE that hydrolyzes both **cAMP** and **cGMP (Fujishige *et al.*, 1999; Soderling *et al.*, 1999), and it is highly** enriched **in the central nervous system (CNS) of many mammalian species including humans (Coskran *et al.*, 2006; Seeger *et al.*, 2003).** In the mammalian brain, PDE10A mRNA and protein are selectively expressed in striatal medium spiny neurons (MSNs) (Bender and Beavo, 2006; Coskran *et al.*, 2006; Fujishige *et al.*, 1999; Seeger *et al.*, 2003).

The striatal outputs mediated by MSNs are divided into two pathways: the dopamine D_2 receptor expressing indirect pathway and the D_1 receptor expressing direct pathway (Graybiel, 1990, 2000). Activation of the indirect pathway by D_2 receptor antagonism is thought to be the principal mechanism of action of most antipsychotic drugs (Karam *et al.*, 2010); however, excessive activation of the indirect pathway by D_2 receptor antagonists is known to cause extrapyramidal symptoms (EPS) (Krebs *et al.*, 2006). Activation of the direct pathway is expected to counteract excessive activation of the indirect pathway and reduce these side

effects (Siuciak *et al.*, 2006). In line with this idea, PDE10A inhibitors have shown lower risks of EPS through the activation of both direct and indirect pathways in pre-clinical studies (Grauer *et al.*, 2009). In addition to EPS, some of the current antipsychotics cause hyperprolactinemia owing to their D_2 receptor antagonism in the pituitary gland (Rourke *et al.*, 2006). PDE10A inhibitors can avoid hyperprolactinemia as PDE10A expression is low in the pituitary gland. Furthermore, PDE10A inhibitor can modulate cognitive functions via activation of corticostriatal circuit (Graybiel, 2000; Simpson *et al.*, 2010). Accordingly, **PDE10A inhibition** can be a novel therapeutic approach for the treatment of schizophrenia with lower risks of these side effects (Kehler and Nielsen, 2011; Menniti *et al.*, 2007; Siuciak *et al.*, 2006). Moreover, several pre-clinical studies have shown that PDE10A inhibitors can protect striatal MSNs against neurodegeneration in Huntington's disease (HD) models through the improvement of cAMP signaling (Giampà *et al.*, 2010; Giampà *et al.*, 2009; Kleiman *et al.*, 2011). Thus, I decided to develop a PDE10A inhibitor as a therapeutic drug for the abovementioned CNS disorders.

Each PDE family has essential functions; thus, PDE10A selectivity is critical for avoiding off-target effects associated with inhibition of other PDEs. For instance, PDE4 inhibition in the brainstem is thought to cause emesis (Mori *et al.*, 2010), and PDE6 inhibition in the mammalian retina can cause disturbance in visual function (Cote, 2004). PDE10A selectivity is also crucial in understanding the pharmacological profile of PDE10A inhibitors because

small molecules targeting distinct PDEs show overlapping pharmacological effects. For example, both the PDE4 inhibitor rolipram and the PDE5 inhibitor zaprinast enhance memory function in novel object recognition test (NORT) using mice (Akar *et al.*, 2014). Both the PDE2 inhibitor BAY 60-7550 and the PDE10A inhibitor PQ-10 attenuate scopolamine- and MK-801-induced memory deficits in NORT using rats (Reneerkens *et al.*, 2013). In addition, the PDE4 inhibitor RO 20-1724, the PDE5 inhibitor sildenafil, and the PDE10 inhibitor TP-10 ameliorate motor dysfunction in rodent HD models (Giampà *et al.*, 2010; Thakur *et al.*, 2013). Thus, careful validation of PDE10A selectivity under physiological conditions is crucial for the precise profiling of PDE10A inhibitors.

Cmpd-A

[1-[2-fluoro-4-(1*H*-pyrazol-1-yl)phenyl]-5-methoxy-3-(1-phenyl-1*H*-pyrazol-5-yl)-pyridazin-4(1*H*)-one] was discovered as a novel PDE10A inhibitor by optimization using a structure-based drug design strategy (Kunitomo *et al.*, 2014). In the present study, I investigated the PDE10A selectivity of Cmpd-A using multiple methods, including *in vitro* and *in vivo* autoradiography (ARG) in rodents. Finally, I assessed PDE10A occupancy by Cmpd-A in rats using T-773 as a tracer; [^{11}C]T-773 is our original PET radioligand for PDE10A (Harada *et al.*, 2015b). Translational studies with Cmpd-A based on the information presented here will help us to understand the pharmacological profile of PDE10A inhibitors as potential CNS drugs.

Materials and Methods

Ethics Statement

The care and use of the animals and the experimental protocols used in this research were approved by the Experimental Animal Care and Use Committee of Takeda Pharmaceutical Company Limited.

Animals

Seven-week-old male Sprague–Dawley (SD) rats were purchased from **Charles River** Laboratories **Japan, Inc**. (Yokohama, Japan). After acclimation for 1 week in our laboratory, the 8-week-old rats were used for experiments. *Pde10a* wild-type (WT) and homozygous knockout (KO) mice (129/SvEv-C57BL/6) were purchased from Taconic Farms, Inc. (Hudson, NY), and used for experiments after at least 1 week of acclimation. The animals were housed in a light-controlled room (12-h light/dark cycle with lights on from 7:00 AM). Food and water were provided *ad libitum*.

Radioligands and Chemicals

Cmpd-A, MP-10 succinate, and T-773 were synthesized by Takeda Pharmaceutical Company Limited. MP-10 has been reported to be a potent and selective PDE10A inhibitor developed by Pfizer Inc. (New York City, NY) (Grauer *et al.*, 2009; Schmidt *et al.*, 2008;

Verhoest *et al.*, 2009). [^{3}H]Cmpd-A (37.0 MBq/mL in ethanol) was synthesized by Sekisui Medical Co., Ltd. (Tokyo, Japan). The specific radioactivity and radiochemical purity were 665 GBq/mmol and 98.1%, respectively. [^{14}C]Cmpd-A was synthesized by Nemoto Science Co., Ltd. (Tokyo, Japan). The specific radioactivity and radiochemical purity were 3.08 GBq/mmol and 99.2%, respectively. [^{3}H]T-773 (37.0 MBq/mL in ethanol) was synthesized by Quotient Bioresearch (Radiochemicals) Limited (Cambridgeshire, UK). The specific radioactivity and the radiochemical purity were 555 GBq/mmol and 99.9%, respectively.

Preparation of Tissue Slices

Male SD rats and male *Pde10a* WT and KO mice were euthanized by decapitation. The brains were rapidly removed, slowly frozen in an isopentane-dry ice bath, and then stored in a deep freezer. Sagittal or coronal 20-µm-thick sections were cut in a cryostat (Leica Microsystems, Wetzlar, Germany) and thaw-mounted onto glass slides. For the rat, coronal brain sections were collected from the region between 1.7 to 0.2 mm anterior to bregma, and sagittal sections were collected from the region 1.9–3.4 mm lateral to the midline (Paxinos and Watson, 1998). For the mouse, coronal brain sections were collected from the region between 1.5 to 0.7 mm anterior to bregma (Paxinos and Franklin, 2001).

***In Vitro* ARG Using Rat and Mouse Brain Sections**

Sagittal brain sections prepared from a rat brain or coronal brain sections prepared from *Pde10a* WT and KO mouse brains (n=5 per genotype) were warmed to room temperature (RT). The sections were pre-incubated in buffer (50 mM Tris-HCl pH 7.5, 1.7 mM EDTA, 6 mM $MgCl_2$, 120 mM NaCl and 0.1% BSA) twice for 5 min at RT. The sections were then incubated in binding buffer (pre-incubation buffer containing 0.03% Triton X-100) with [^{3}H]Cmpd-A (8 nM for rats and 16 nM for mice) or [^{3}H]T-773 (20 nM for rats) for 60 min at RT. Blocking of specific binding in adjacent sections was conducted by the addition of an excess amount of PDE10A-selective inhibitors to the radioligand-containing buffer (final concentration of 1 μM). The sections were washed twice for 5 min ([^{3}H]Cmpd-A) or for 1 min ([^{3}H]T-773) at 4°C in pre-incubation buffer, and then rapidly rinsed in ice-cold distilled water. The sections were dried under a stream of cool air, and were exposed to BAS IP TR 2040E imaging plates (GE Healthcare UK Ltd.) for 5–7 days. The imaging plates were analyzed using an image analyzer FLA-7000 (Fujifilm, Tokyo, Japan) and image analyzing software ImageGauge 4.0 (Fujifilm). In the ARG study using [^{3}H]Cmpd-A, regions of interest (ROIs) were placed at the frontal cortex (Fcx), caudate putamen (CPu), nucleus accumbens (NAc), thalamus (Thal), brainstem (Bs), hippocampus (Hipp), and cerebellum (Cb). Radioactivity in each ROI was analyzed and represented as photostimulated luminescence (PSL) values. The background was subtracted from the PSL values of each ROI, and the PSL values in each brain region were then averaged for each group. In the ARG study in mouse

brain sections, the PSL values in the presence and absence of an excess amount of MP-10 were represented as total binding and non-specific binding (NSB), respectively. The rat brain sections adjacent to those used for ARG were stained with hematoxylin and eosin (HE) for anatomical identification.

Saturation Binding Assay with [^{3}H]Cmpd-A Using Rat Brain Sections

Coronal brain sections prepared from 4 rat brains were warmed to RT, and were pre-incubated twice in buffer for 5 min at RT. The sections were then incubated with 0.25, 0.5, 1, 2, 4, 8, 16, or 32 nM [^{3}H]Cmpd-A in binding buffer for 60 min at RT. NSB was determined in the presence of 1 μM MP-10. The sections were rinsed, dried using the same procedure described above, and then exposed to an imaging plate for 6 days. Autoradiograms were read using FLA-7000 and analyzed using ImageGauge 4.0. ROIs were placed at the CPu and NAc shell of both hemispheres in each section and radioactivity in the ROIs was represented as PSL values. The background PSL value was subtracted from the PSL values of each ROI, and the PSL values of the left and right hemispheres were averaged for each section. The PSL values in the absence and presence of an excess amount of MP-10 were represented as total binding and NSB, respectively. The saturation binding curves were fit by nonlinear regression using GraphPad Prism 5.01 (GraphPad Software, Inc., La Jolla, CA), and the dissociation constant (K_d value) was calculated using the same software.

In Vivo ARG with [^{14}C]Cmpd-A in Rats

[^{14}C]Cmpd-A was suspended in 0.5% (w/v) methylcellulose in distilled water and orally administrated to male SD rats (n=2) at 1.5 mg/kg (10.1 MBq/9.48 mL/kg). At 6 h after administration, the rats were euthanized by inhalation of chloroform under anesthesia with isoflurane, and were preliminarily frozen in a bath of dry ice/hexane. The decapitated head was embedded in 2% (w/v) sodium carboxymethyl cellulose in distilled water. Using a cryostat, 40-µm-thick sagittal sections were collected from the right hemispheres of the heads, and then 40-µm-thick coronal sections were collected from the left hemispheres. These sections were freeze-dried in a cryostat at approximately –20°C for 1 day. The sections were then covered with a sample-protecting film (Nakagawa Mfg. Co., Ltd., Warabi, Japan) and were exposed to an imaging plate BAS-MS2040 or BAS-III2040 (GE Healthcare UK Ltd.) for 48 h. After the exposure, the imaging plate was analyzed with an image analyzer FLA-7000 (Fujifilm).

In vivo Occupancy Study of Cmpd-A in Rats

Cmpd-A was suspended in 0.5% (w/v) methylcellulose in distilled water, and T-773 was dissolved in *N*,*N*-dimethylacetamide and 1,3-butanediol (1:1). Cmpd-A (0, 0.03, 0.1, 0.3, 1, 3, and 10 mg/kg) was orally administered to male SD rats (n=2-3 in each group), and 0.02

mg/kg of T-773 was administered by bolus intravenous injection via the lateral tail vein 90 min after Cmpd-A administration. The rats were anesthetized by inhalation of 4% isoflurane and were euthanized by cardiac perfusion with heparinized saline 30 min after T-773 injection, and the whole brains were isolated. The striatum (Str) and cerebellum (Cb) were dissected from the brains, and were stored at −30°C until use. The frozen samples were homogenized in saline at 4 mL/g tissue, and the concentration of T-773 was measured by mass spectrometry (MS) in each homogenate. Specific T-773 binding (B_{SP}) in Str was represented as the difference between the T-773 concentration in Str and that in Cb. PDE10A occupancy was calculated using the following equation: Occupancy (%) = $(B_{SP,base} - B_{SP,drug})/B_{SP,base} \times 100$, where $B_{SP,base}$ and $B_{SP,drug}$ are the concentrations at baseline (vehicle-treatment) and at drug-treatment, respectively. The saturation curve of occupancy was fit by nonlinear regression using GraphPad Prism 5.02.

Results

In Vitro PDE10A Selectivity of Cmpd-A

Cmpd-A was identified as a novel PDE10A inhibitor. I have reported the PDE10A2 inhibitory activity of Cmpd-A and its selectivity over other PDE family enzymes by *in vitro* enzyme inhibition assays using various human recombinant PDE family proteins (Kunitomo *et al.*, 2014). The half-maximal inhibitory concentration (IC_{50}) value of Cmpd-A for PDE10A2 was 0.30 nM, and the minimum IC_{50} value among the other 10 PDE families was 5500 nM for PDE4D2. Thus, the PDE10A2 selectivity of Cmpd-A over other PDE family enzymes was more than 15000-fold. *In vitro* PDE10A2 selectivity of Cmpd-A was further assessed by measuring its inhibitory or stimulatory activities against enzymes (Table 1) and receptors (Table 2) at Ricerca Biosciences (Concord, OH). More than 50% inhibition or stimulation by 10 μM of Cmpd-A was considered as a significant response. Cmpd-A did not induce a significant response in 91 target molecules, except for PDEs. These results indicate that Cmpd-A is a potent and selective inhibitor of human PDE10A *in vitro*.

In Vitro ARG with [^{3}H]Cmpd-A in Rat Brain Sections

To confirm the selectivity of Cmpd-A for native PDE10A, *in vitro* ARG with [^{3}H]Cmpd-A was performed using rat brain sagittal sections. The chemical structure of [^{3}H]Cmpd-A is shown in Fig. 2A. For anatomical identification, HE staining was conducted using adjacent

sections (Fig. 2B). The radioactivity of [^{3}H]Cmpd-A was selectively detected in the CPu, NAc, the globus pallidus (GP), and the substantia nigra (SN), where PDE10A is highly expressed. Radioactivity was also detected in the connecting pathway between the striatal complex and SN (Fig. 2C). Following this, I investigated the inhibition of [^{3}H]Cmpd-A accumulation by using PDE10A inhibitors with different chemical structures: MP-10 and non-radiolabeled Cmpd-A. The selective accumulation of [^{3}H]Cmpd-A at 8 nM was mostly blocked by 1 μM of either MP-10 or Cmpd-A (Fig. 2D and E). The amount of [^{3}H]Cmpd-A radioactivity in several brain regions in the absence or presence of these cold compounds was represented as PSL value (/mm^2) (Fig. 2F). In the presence of 1 μM of MP-10, [^{3}H]Cmpd-A radioactivity was significantly decreased in the CPu ($P \leq 0.01$), NAc ($P \leq 0.01$), and Hipp ($P \leq 0.05$). The PSL values in the presence of 1 μM of MP-10 were considered as backgrounds and the specific binding of [^{3}H]Cmpd-A in the CPu, NAc, and Hipp was calculated using these PSL values. High specific binding was observed in the CPu and NAc with PSL values of 175 ± 21.3 and 88.2 ± 20.1, respectively. The PSL value in the Hipp was only 4.26 ± 0.784, which was more than 40-fold lower than that in the CPu. These results suggest that [^{3}H]Cmpd-A selectively binds to native PDE10A in rat brain sections.

In Vitro ARG with [^{3}H]Cmpd-A in Mouse Brain Sections

I next performed *in vitro* ARG using [^{3}H]Cmpd-A and coronal brain sections from *Pde10a* WT and KO mice. In WT mouse brain sections, [^{3}H]Cmpd-A selectively accumulated in the CPu and NAc, where PDE10A is highly expressed (Fig. 3A). This selective accumulation was not observed in brain sections from *Pde10a* KO mice (Fig. 3B). I also conducted a blocking experiment with an excess amount of MP-10 (1 μM) using brain slices from these mice. In the presence of 1 μM of MP-10, [^{3}H]Cmpd-A radioactivity in the CPu of WT mouse brain sections was similar to that in KO mouse brain sections (Fig. 3C). These results further demonstrate the specific binding of [^{3}H]Cmpd-A to native PDE10A.

Binding Affinity of [^{3}H]Cmpd-A for Native PDE10A in Rat Brain Sections

I next evaluated the binding affinity of [^{3}H]Cmpd-A to native PDE10A. I conducted a saturation binding assay using rat brain coronal sections and calculated K_d values in the CPu and the shell region of NAc. ROIs in a rat brain section were shown in Fig. 4A. Selective and saturable binding of [^{3}H]Cmpd-A was observed in these regions with mean ± SEM K_d values of 7.2 ± 1.2 nM for the CPu and 2.6 ± 0.5 nM for the NAc shell (Fig. 4B and C), suggesting that [^{3}H]Cmpd-A binds to a single high-affinity site of PDE10A in the rat brain.

***In Vivo* ARG with [^{14}C]Cmpd-A in Rats**

To validate PDE10A selectivity of Cmpd-A *in vivo, in vivo* ARG was conducted after oral administration of [^{14}C]Cmpd-A. The chemical structure of [^{14}C]Cmpd-A is shown in Fig. 5A. Six hours after oral administration of [^{14}C]Cmpd-A (1.5 mg/kg), autoradiograms of sagittal and coronal head sections were obtained. High radioactivity was observed in the CPu, NAc, GP, and SN of the rat brain regions (Fig. 5B-H), consistent with those in which [^{3}H]Cmpd-A accumulated in *in vitro* ARG studies and with areas of PDE10A high expression in the rat brain. Thus, [^{14}C]Cmpd-A appears to selectively bind to native PDE10A protein *in vivo*.

In Vivo Occupancy Study of Cmpd-A in Rats

PDE10A occupancy by Cmpd-A was measured using T-773 as a tracer. First, I investigated whether Cmpd-A could compete with PDE10A-selective binding of T-773. [^{3}H]T-773 selectively accumulated in PDE10A-expressing regions in sagittal brain sections (Fig. 6A), and the accumulation was almost completely blocked in the presence of an excess amount of Cmpd-A (Fig. 6B), indicating binding competition between [^{3}H]T-773 and Cmpd-A.

In vivo occupancy study using non-radiolabeled tracer is an established method which confers several advantages over those using radiolabeled tracers in living animals, such as no risk of contamination by radionuclides and no influence of radiometabolites (Chernet *et al.*, 2005; Nirogi *et al.*, 2012). Therefore, PDE10A occupancy by Cmpd-A was measured using non-radiolabeled T-773 as a tracer. Specific binding of T-773 to PDE10A in the Str was

calculated using the Cb as a reference region based on the lack of specific binding of [^{3}H]Cmpd-A (Fig. 2); amount of T-773 that specifically bound to PDE10A in the Str was determined by taking the difference in its concentration between the Str and Cb. Striatal PDE10A occupancy by Cmpd-A was calculated from the reduction in the binding amount of T-773 to PDE10A after administration of various dosage of Cmpd-A. The Tmax of orally administered Cmpd-A in the rat brain was 2 h in our preliminary study. Therefore, non-radiolabeled T-773 was intravenously injected to rats 90 min after oral administration of Cmpd-A, and then the Str and Cb were collected from each rat 30 min after T-773 injection. The striatal concentration of T-773 without Cmpd-A administration was more than 5-fold higher than that of the reference area, Cb, suggesting the Str-selective accumulation of T-773 (Table 3). The concentration of T-773 in the Str was dose-dependently decreased by pretreatment with Cmpd-A (Table 3). When the Cb was employed as a reference site, the calculated PDE10A occupancy by Cmpd-A in the Str was increased in a dose-dependent manner (Fig. 6C). When data were fitted by nonlinear regression, PDE10A occupancies at 0.3 and 3 mg/kg of Cmpd-A were 26% and 77%, respectively. Cmpd-A (0.88 mg/kg) was estimated to produce 50% PDE10A occupancy within the Str.

Discussion

Cmpd-A showed potent inhibitory activity (IC_{50} value of 0.30 nM) and high selectivity (more than 15000-fold against other PDEs) for human recombinant PDE10A2 *in vitro* (Kunitomo *et al.*, 2014). Moreover, Cmpd-A did not induce a significant response when tested for activity against 91 enzymes and receptors except for PDE family even at 10 μM, which is more than a 33000-fold higher concentration than the IC_{50} value for recombinant PDE10A2 (0.30 nM). Thus, Cmpd-A is highly selective for recombinant PDE10A *in vitro*.

I performed ARG using radiolabeled Cmpd-A and rodent brain sections to confirm the selectivity of Cmpd-A for native PDE10A. PDE10A is highly enriched in striatal MSNs (Siuciak *et al.*, 2006). MSNs constitute the direct and indirect pathways projecting to the SN and GP, respectively (Lei *et al.*, 2004). High levels of accumulation of [^{3}H]Cmpd-A were observed in the CPu, NAc, GP, SN, and the striatonigral projection of the rat brain, supporting the selective accumulation of [^{3}H]Cmpd-A in striatal MSNs. MP-10 was previously reported to interact with PDE10A at the substrate-binding site in the catalytic domain (Verhoest *et al.*, 2009). Co-crystal structural analysis of Cmpd-A with the PDE10A catalytic domain showed that Cmpd-A also uses this binding site (Kunitomo *et al.*, 2014). Therefore, I performed a blocking study using MP-10 as a control to confirm PDE10A-selective binding of [^{3}H]Cmpd-A in an *in vitro* ARG study. As expected, [^{3}H]Cmpd-A accumulation in rat brain sections was almost entirely blocked by an excess amount of either non-radiolabeled Cmpd-A

or MP-10. Furthermore, the Str-selective accumulation of [^{3}H]Cmpd-A was almost completely abolished in brain sections from *Pde10a* KO mice with complete deletion of PDE10A protein (Harada *et al.*, 2015b). These results indicate the PDE10A-specific binding of Cmpd-A under physiological conditions.

In previous immunohistochemical studies with rat brain sections, PDE10A immunoreactivity was detected in parts of the Hipp, Cb, and cortex, as well as the CPu, NAc, GP, and SN (Coskran *et al.*, 2006; Seeger *et al.*, 2003). In those reports, PDE10A expression was confined to individual neuronal nuclei in the Hipp, Cb, and cortex. PDE10A expression levels were 50–200-fold lower in the Hipp, Cb, and cortex than that in the Str (Coskran *et al.*, 2006; Seeger *et al.*, 2003). In the present autoradiography study, specific binding of [^{3}H]Cmpd-A in the Hipp was observed at more than 40-fold lower levels than that in the CPu, and no specific binding was observed in the Fcx, Thal, Bs, and Cb. Thus, PDE10A may be expressed in the Hipp at more than 40-fold lower levels than that in the CPu. PDE10A expression levels in the other non-striatal regions are under detection limit at the level of sensitivity of the present study.

A saturation binding assay using rat brain sections showed that [^{3}H]Cmpd-A bound to a single high-affinity binding site with K_d values of 7.2 and 2.6 nM in the CPu and NAc shell, respectively. It is reasonable to determine NSB by the addition of 1 μM of MP-10 because this concentration of MP-10 almost completely inhibited the selective binding of [^{3}H]Cmpd-A in

the blocking study. Indeed, [^{3}H]Cmpd-A binding in the presence of 1 μM of MP-10 was linear in both the CPu and NAc shell over the range of concentrations used, suggesting NSB. As discussed before, the Cmpd-A-binding site in the PDE10A enzyme is the substrate-binding site in the catalytic domain; thus, the high binding affinity of Cmpd-A suggests potent inhibitory activity against native PDE10A.

Orally administered [^{14}C]Cmpd-A selectively accumulated in rat brain areas associated with high PDE10A expression in the *in vivo* ARG study. This result suggests that systemically administered Cmpd-A can penetrate the blood-brain barrier and specifically bind to native PDE10A in living rats. I measured PDE10A occupancy by Cmpd-A using T-773, a brain penetrable PDE10A-specific tracer, with the Cb as a reference region (Harada *et al.*, 2015b). The *in vitro* competitive binding study revealed that PDE10A-selective accumulation of [^{3}H]T-773 can be inhibited by Cmpd-A; thus, PDE10A occupancy by Cmpd-A can be measured using T-773 displacement. Fitted by nonlinear regression, a dose of 0.88 mg/kg of Cmpd-A was estimated to produce 50% PDE10A occupancy within the striatum.

In summary, I demonstrated that Cmpd-A is specific for both recombinant PDE10A *in vitro* and for native PDE10A *in vivo*. Furthermore, PDE10A occupancy of orally administered Cmpd-A was successfully calculated using T-773 as a tracer in rats. Pre-clinical and clinical investigations of the therapeutic potential of Cmpd-A against CNS disorders such as schizophrenia and HD with accurate information regarding PDE10A occupancy will improve

our understanding of the relation between enzyme occupancy and the pharmacodynamic effects of PDE10A inhibitors and provide important information regarding this translational approach.

Part 2

Specific Inhibition of Phosphodiesterase 10A Protects from Striatal Neurodegeneration and Ameliorates Behavioral Deficits in the R6/2 Mouse Model of Huntington's Disease

Abstract

Huntington's disease (HD) is characterized by progressive loss of striatal medium spiny neurons (MSNs) that constitute direct and indirect pathways: the indirect pathway MSNs is more vulnerable than the direct pathway MSNs. Impairment of cAMP/cGMP signaling by mutant huntingtin is hypothesized as the molecular mechanism underlying degeneration of MSNs. Phosphodiesterase 10A (PDE10A) is selectively expressed in MSNs and degrades both cAMP and cGMP; thus, PDE10A inhibition can restore impaired cAMP/cGMP signaling. Compared with other PDE10A inhibitors, a novel PDE10A inhibitor Cmpd-A [1-[2-fluoro-4-(1H-pyrazol-1-yl)phenyl]-5-methoxy-3-(1-phenyl-1H-pyrazol-5-yl)pyridazin-4 (1H)-one] showed comparable activation of the indirect pathway MSNs, while it produced partial activation of the direct pathway MSNs by its faster off-rate property. Here, I report the effects of Cmpd-A on striatal neurodegeneration and behavioral deficits in the R6/2 mouse model of HD. Cmpd-A at 0.5 or 5 mg/kg/day was orally administrated from 4.5–5 to 12 weeks of age, and the effects of Cmpd-A were characterized over this period. Repeated treatment with Cmpd-A suppressed the reduction of brain-derived neurotrophic factor levels, prevented striatal neurodegeneration, and suppressed increase in seizure frequency, but did not prevent the suppression of body weight gain. As for motor deficits, Cmpd-A suppressed the development of clasping behavior and motor dysfunctions, including decreased motor activity in the open field, but did not improve the impairment in motor coordination on the

rotarod. Regarding cognitive functions, Cmpd-A improved deficits in procedural learning, but was ineffective for deficits in contextual memory. These results suggest that Cmpd-A reduces striatal neurodegeneration and ameliorates behavioral deficits in R6/2 mice.

Introduction

Huntington's disease (HD) is an autosomal dominant, inherited neurodegenerative disease associated with progressive cognitive impairment and motor symptoms such as chorea, akinesia, and dystonia (Ross and Tabrizi, 2011; Walker, 2007). HD is caused by a mutation that results in an abnormal expansion of cytosine-adenine-guanine (CAG) trinucleotide repeats beyond about 35 repeats within exon 1 of the huntingtin gene, which encodes the huntingtin protein (Frank, 2014; Ross *et al.*, 2014; Walker, 2007). Although mutant huntingtin is expressed throughout the brain, the most prominent cell loss is of medium spiny neurons (MSNs) in the striatum (Vonsattel and DiFiglia, 1998). The MSNs constitute two distinct output pathways: the direct and indirect pathways (Graybiel, 1990, 2000). Particularly, indirect pathway MSNs appear to be more vulnerable to degeneration than direct pathway MSNs in patients with HD (Galvan *et al.*, 2012; Glass *et al.*, 2000; Reiner *et al.*, 1988; Sapp *et al.*, 1995). So far, multiple animal models of HD have been established (Pouladi *et al.*, 2013). HD model mice, such as R6/2, CAG140 and YAC128 mice, are initially hyperactive and gradually become hypoactive (Lüesse *et al.*, 2001; Menalled *et al.*, 2003; Slow *et al.*, 2003), suggesting the reduced output from both direct and indirect pathway MSNs. Those phenotypes might reflect the higher vulnerability of indirect pathway MSNs than direct pathway MSNs at earlier phases, although the direct evidence is limited. Interestingly, green fluorescent protein, selectively expressed in indirect pathway MSNs under Drd2 promoter

control, was reduced from early stages of disease progression in R6/2, R6/1, CAG140, and HdhQ111 mice (Crook and Housman, 2012). Those HD model mice might not completely replicate the HD pathology; however, these mice would be useful for preclinical evaluation of potential therapeutics for the treatment of HD. Impairment in cAMP signaling and its downstream cAMP response element-binding protein (CREB) signaling pathway by mutant huntingtin protein has been hypothesized to play a critical role in the neurodegeneration in HD pathology (Choi *et al.*, 2009; Gines *et al.*, 2003; Mantamadiotis *et al.*, 2002; Nucifora *et al.*, 2001; Sugars and Rubinsztein, 2003; Wyttenbach *et al.*, 2001). Neuronal nitric oxide synthase mRNA is also decreased in the postmortem striatum of patients with HD (Norris *et al.*, 1996), suggesting the downregulation of cGMP signaling. Thus, activation of cAMP and cGMP signaling pathways, especially in indirect pathway MSNs, could be a potential therapeutic approach for HD.

Phosphodiesterase 10A (PDE10A) is a dual-substrate PDE that hydrolyzes both cAMP and cGMP, and is highly expressed in both direct and indirect pathway MSNs (Coskran *et al.*, 2006; Fujishige *et al.*, 1999; Seeger *et al.*, 2003). PDE10A inhibitors activate both types of MSNs, and previous studies suggested the indirect pathway preferential activation by PDE10A inhibitors such as papaverine, TP-10, and MP-10 (Nishi *et al.*, 2008; Threlfell *et al.*, 2009; Wilson *et al.*, 2015). A selective PDE10A inhibitor TP-10 significantly increased striatal cell survival and activated CREB in the quinolinic rat model of HD (Giampà *et al.*,

2009). TP-10 also showed significant beneficial effects in R6/2 mice; it recovered striatal and cortical levels of phosphorylated CREB and BDNF, inhibited striatal atrophy, and showed improvement in clasping behavior, performance in rotarod, and locomotor activity (Giampà *et al.*, 2010). TP-10 was reported to increase the corticostriatal transmission via upregulation of cGMP signaling (Padovan-Neto *et al.*, 2015), which might also contribute to its beneficial effects in the quinolinic rat model and R6/2 mice. Thus, restoring cAMP and cGMP signaling by PDE10A inhibition may be a promising treatment approach for HD. Cmpd-A [1-[2-fluoro-4-(1H-pyrazol-1-yl)phenyl]-5-methoxy-3-(1-phenyl-1H-pyrazol-5-yl)-pyridazin-4(1H)-one] is a selective and orally active PDE10A inhibitor (Kunitomo *et al.*, 2014). Interestingly, our previous study revealed that activation pattern of MSNs by a faster off-rate PDE10A inhibitor Cmpd-A was different from those by slower off-rate PDE10A inhibitors such as MP-10 and compound 1; compared to MP-10 and compound 1, Cmpd-A equally activated indirect pathway MSNs, whereas it partially activated direct pathway MSNs (Suzuki *et al.*, 2016)**.** Considering the lower vulnerability of direct pathway MSNs than that of indirect pathway MSNs, this MSN activation pattern by Cmpd-A could protect MSNs in both pathways from neurodegeneration by mutant huntingtin without unbalanced activation of these pathways.

In this study, I investigated the effects of Cmpd-A on the R6/2 mouse model of HD. R6/2 mouse line is a widely used transgenic (Tg) mouse model of HD with several phenotypes

similar to that seen in patients with HD, including striatal atrophy, motor deficits, and cognitive impairments. Here, I report preclinical evidence that Cmpd-A protects from striatal neurodegeneration and ameliorates behavioral deficits in R6/2 mice.

Materials and Methods

Ethics Statement

All behavioral studies were conducted by PsychoGenics Inc. (Tarrytown, NY) according to principles of the Public Health Service Policy on Humane Care and Use of Laboratory Animals, and procedures were approved by the Institutional Animal Care and Use Committee of PsychoGenics Inc. (IACUC protocol number: 179_0312). PsychoGenics Inc. achieved Association for Assessment and Accreditation of Laboratory Animal Care International accreditation (AAALAC Unit #001213).

Animals

R6/2 Tg mice carrying the N-terminal region of a mutant human huntingtin gene and wild-type (WT) mice were used in this study (Mangiarini *et al.*, 1996). Mice were bred in the colony of PsychoGenics Inc. by crossing ovarian transplanted females on a CBA×C57BL/6 background (The Jackson Laboratory, Bar Harbor, ME) with male C57BL/6 mice. Mice were identified before weaning by real-time PCR of tail snips. CAG repeat length in mutant mice was analyzed by ABI Prism 377 DNA Sequencer (Life Technologies, Carlsbad, CA). Average CAG repeat lengths for each R6/2 mouse group were as follows: vehicle-treated group, 123.79 ± 0.35; 0.5 mg/kg/day of Cmpd-A–treated group, 123.34 ± 0.48; 5 mg/kg/day of Cmpd-A–treated group, 123.66 ± 0.49 (mean ± SEM; n = 19–22). Mice were given 1-min

handling habituation on 2 consecutive days between 19–21 days of age, and were identified by tail tattoo at 20–21 days of age and weaned at 21–22 days of age. Mice were housed in a room with light control (12-h light/12-h dark cycle with lights on at 7:00 AM). Food and water were provided *ad libitum*. Animals were checked for survival twice per day and body weighed once per week. Mice from multiple littermates were used for each treatment group (almost equally divided between sexes), and housed 4–5 mice/cage. Two WT mice of the same sex, but different littermates, were included in each cage for providing normal social stimulation.

Chemicals

Cmpd-A

[1-[2-fluoro-4-(1*H*-pyrazol-1-yl)phenyl]-5-methoxy-3-(1-phenyl-1*H*-pyrazol-5-yl)-pyridazin-4(1*H*)-one] was synthesized by Takeda Pharmaceutical Company Limited (Fujisawa, Japan). Cmpd-A was suspended in vehicle (0.5% methylcellulose in sterile water) using an ultrasonic sonicator for 10 min and was then mixed by pipetting and inverting the tube to eliminate any precipitation. Dosing solutions were formulated daily. All formulated dosing solutions were prepared in amber glass vials. The formulated solutions were additionally stirred for at least 10 min before dosing and were stirred throughout the dosing session. Daily oral administration of vehicle or Cmpd-A at 0.5 mg/kg or 5 mg/kg with a dose volume of 10

mL/kg was started from 4.5–5 to 12 weeks of age. The drugs were administered after the completion of behavioral tests each day. No mice were dead up to 12 weeks of age.

Biochemical Analysis

At 12 weeks of age (after 8 weeks of repeated dosing and behavioral studies), mice (n = 6 in each group) were sacrificed and tissue collected 3 h after the last administration. Plasma samples of Cmpd-A-treated groups were also collected at the same time point. The plasma concentrations of Cmpd-A at 0.5 and 5 mg/kg/day were 191.2 ± 11.0 and 1123.5 ± 32.5 ng/mL, respectively (mean ± S.E.M., n = 7). Striatal PDE10A occupancies of Cmpd-A at plasma concentrations of 191.2 and 1123.5 ng/mL are estimated as 58 and 89%, respectively, in mice (data not shown). The brains were rapidly removed and rinsed in ice cold saline. The striatum and cerebral cortex were then immediately dissected and frozen on dry ice. The dissected tissues were homogenized by ultrasonic sonication in 20 mL/g of lysis buffer (137 mM NaCl, 20 mM Tris-HCl pH 8.0, 1% NP40, 10% glycerol, and 1% proteinase inhibitor cocktail). The homogenates were centrifuged at 15,000 rpm for 20 min at 4°C, and the supernatants were frozen at −80°C until use. Brain-derived neurotrophic factor (BDNF) levels were determined using BDNF $E_{max}^{®}$ ImmunoAssay System kit (Promega, Madison, WI) following the manufacturer's instructions. The 96-well plates coated with anti-BDNF monoclonal antibody were incubated with a blocking buffer at room temperature (RT) for 1 h.

The frozen samples and BDNF standards were applied to the plates. The plates were incubated with shaking for 2 h at RT, followed by rinse with the washing buffer. Then, the plates were incubated with anti-BDNF polyclonal antibody for 2 h at RT, and were rinsed with the washing buffer. The plates were incubated with horseradish peroxidase-conjugated anti-IgY antibody for 1 h at RT. To produce a color reaction, the solution of peroxidase substrate and tetramethylbenzidine was added to the plates. The reaction was terminated by addition of 1 M hydrochloric acid, and then the absorbance was measured at 450 nm using a plate reader Wallac ARVO SX 1420 (PerkinElmer, Waltham, MA).

Histochemical Analysis

At 12 weeks of age (after 8 weeks of daily dosing and behavioral studies), mice (n = 4 in each group, 2 males and 2 females) were randomly selected and were anesthetized with sodium pentobarbital and transcardially perfused with saline, followed by 4% paraformaldehyde in 0.1 M phosphate buffered saline (PBS) 3 h after the last administration. The whole brain was removed and fixed overnight in 4% paraformaldehyde in 0.1 M PBS at 4°C and then transferred to a solution of 30% sucrose in 0.1 M PBS at 4°C. The brains were embedded in 7.5% sucrose containing Tissue-Tek OCT Compound (Sakura Finetek, Tokyo, Japan) and were stored at −80°C until use. Multiple coronal serial sections per animal (20 μm thick) within the coordinates of 0.86–0.50 mm rostrocaudal from bregma, were cut on a

cryostat. Two sections per animal were randomly selected from the multiple sections for the following staining. Cresyl violet (MP Biomedicals, Aurora, OH) was used to stain Nissl substance in the cytoplasm of neurons. The sections were rehydrated through graded alcohols and then stained with 0.07% acetic acid containing 0.25% aqueous solution of cresyl violet for 30 min. The sections were briefly rinsed with water, followed by dehydration in graded alcohols. The sections were cleared in xylene and were sealed by coverslips. Images of stained sections were captured at ×20 magnification by a slide scanner (NanoZoomer, Hamamatsu Photonics, Hamamatsu, Japan). To assess striatal atrophy, the bilateral striata of the sections were manually delineated according to the stereotaxic atlas of the mouse brain (Paxinos and Franklin, 2001) using NDP viewing software (Hamamatsu Photonics) by an investigator blind to the treatment groups. The defined striatal areas (mm^2) were automatically calculated by the same software. The bilateral striatal areas were averaged between two sections per animal, and further averaged over each treatment group (n = 4).

Experimental Design of Behavioral Study

All testing and assessments were performed during the animals' light cycle phase. Mice in their home cages were transferred from the rearing room to the experimental rooms and were acclimated to the experimental rooms for at least 1 h before the beginning of any experiments. At 4 weeks of age, mice were tested for rotarod and open field behaviors for validation of

baseline phenotypes. Mice were balanced between four treatment groups (vehicle-treated WT mice, vehicle-treated R6/2 mice, 0.5 mg/kg/day of Cmpd-A–treated R6/2 mice, and 5 mg/kg of Cmpd-A–treated R6/2 mice) in terms of sex, body weight, CAG repeat number, and past behavioral performance. Experimenters were blind to both treatment and genotype at time of behavioral testing.

Body Weight

Mice were weighed once per week throughout the study (4–12 weeks of age).

Clasping Behavior

Clasping behavior was weekly assessed at the time body weights were measured. Mice were suspended by the tail for 30 s and observed for hind limb clasping. The percentages of mice showing full clasping behavior within 30 s were calculated at 5–12 weeks of age.

Open Field Test

The open field test was conducted in a Plexiglas square chamber (27.3×27.3×20.3 cm; Med Associates Inc., St. Albans, VT) surrounded by infrared photobeam sources. Horizontal activity (distance traveled) and vertical activity (rearing) were measured by infrared photobeam sources from consecutive beam breaks. Animals were placed in the chambers for

30 min, and total ambulatory distance and total rearing were measured. Mice were tested at 4 (baseline) and 12 weeks of age.

Rotarod Test

Rotarod test was performed over 3 consecutive days at 4 (baseline), 6, and 12 weeks of age. Mice were placed on the rotarod and the speed of rotation was gradually and uniformly increased 4 to 40 rpm over 300 s. The latency to fall off from the rotarod was recorded up to 300 s.

Procedural Water T-Maze Test

To investigate procedural learning and cognitive flexibility, procedural water T-maze test was performed using a T-shaped water maze in mice at 9–10 weeks of age (Menalled *et al.*, 2014; Tanimura *et al.*, 2008). T-maze test was conducted in a room at approximately 15 lux. The black Plexiglas T-maze with arms 33 cm high, 10 cm wide, and 49 cm long was filled with 25 ± 1°C water colored opaque with non-toxic white tempera paint. A platform was submerged approximately 0.5 cm below the water surface at one end of the left or right arm. In the acquisition phase, mice were placed in the stem of the water-filled T-maze and were allowed to swim to find the hidden escape platform in either the right or left arm. The location of the platform was fixed for each mouse. Once a mouse reached the hidden platform, the

mouse was allowed to stay there for 10 s. The mice underwent 8 trials per day with an approximately 15 min of inter-trial interval. If a mouse reached the platform in 6 or more out of 8 trials per day for 2 consecutive days, the mouse met the criteria and the number of days required to meet the criteria was counted. Up to 7 days were provided to achieve the criteria in the acquisition phase and mice that did not reach the criteria within 7 days were assigned a value of 7 (cut-off value). Once the criteria were achieved within 7 days, each mouse was advanced to the reversal phase. In the reversal phase, the platform was located in the opposite arm for each mouse. The performance in this phase was assessed for 6 consecutive days (8 trials per day).

Seizure Susceptibility

Seizures were observed in R6/2 mice during the first 3 days of the acquisition phase when I tried to conduct water T-maze test. These seizures were probably caused by water-immersion stress because R6/2 mice are known to have increased susceptibility to seizures triggered by stress (Mangiarini *et al.*, 1996). The number of observed seizures during those days was counted.

Contextual Fear Conditioning (CFC) Test

To evaluate contextual memory, I conducted a contextual fear conditioning task in mice at

11 weeks of age. Training was performed using an automated software package (Coulbourn, Whitehall, PA). On the training day, mice were acclimated to the testing chamber for 20 s before receiving the first of 5 presentations of 2-s footshock (0.6 mA). The baseline data were recorded during the first shock. The second shock was presented 80 s later; the third and fourth shocks were presented 120 s after the second and third shock, respectively. The final shock was presented 140 s after the fourth shock. Mice were then left in the chambers for 40 s and subsequently returned to their home cages. On the test day, mice were placed back in the original training context for a 3-min period 24 h later from the training. Contextual memory was assessed by measuring a freezing behavior, defined as cessation of all movement with the exception of respiration. Freezing behavior was quantified using software, FreezeFrame (Actimetrics, Wilmette, IL).

Statistical Analysis

The statistical significance of differences between two groups was analyzed using Aspin–Welch test with an alpha level of 0.05. For comparing dose-dependent effects of multiple doses of Cmpd-A with the control group, the homogeneity of variances was assessed by Bartlett's test, and then the statistical significance was analyzed using two-tailed Williams' test (Williams, 1971) (for parametric data, $P > 0.05$ by Bartlett's test) or two-tailed Shirley-Williams test (Shirley, 1977) (for non-parametric data, $P \leq 0.05$ by Bartlett's test).

Differences yielding $P \leq 0.05$ were considered significant. In the clasping test, I scored "1" or "0" when each mouse exhibited full clasping behavior or not, respectively, and the statistical significance was analyzed using two-tailed Shirley-Williams test. In the rotarod test, differences between vehicle-treated WT mice and vehicle-treated R6/2 mice at each week of age were analyzed using a repeated measures analysis of variance (RM-ANOVA) with test day as the repeated factor.

Results

Cmpd-A Suppressed BDNF Reduction in the Striatum of R6/2 Mice.

Cmpd-A dose-dependently increased cAMP and cGMP levels, and upregulated phosphorylation of CREB in the mouse striatum (Suzuki *et al.*, 2015). Cmpd-A at 0.5 mg/kg (51% striatal PDE10A occupancy) significantly increased cAMP and cGMP levels in the mouse striatum after both single and repeated administration (Suzuki *et al.*, 2015; Suzuki *et al.*, 2016). Thus, 0.5 mg/kg and a higher dose (5 mg/kg, 91% PDE10A occupancy in mice) of Cmpd-A were used in this study. Daily oral administration of vehicle or Cmpd-A at 0.5 mg/kg or 5 mg/kg was started from 4.5–5 to 12 weeks of age. Activation of cAMP signaling cascades is known to upregulate BDNF expression via phosphorylation of CREB (Tardito *et al.*, 2006). I evaluated BDNF protein levels in the striatum and the cortex of mice at 12 weeks of age. BDNF levels in the striatum of vehicle-treated R6/2 mice were significantly lower than that of vehicle-treated WT mice ($P \leq 0.01$; Fig. 7A), and 8 weeks of daily treatment with Cmpd-A significantly and dose-dependently suppressed the reduction of BDNF levels in R6/2 mice ($P \leq 0.05$; Fig. 7A). BDNF levels in the cortex of vehicle-treated R6/2 mice were not statistically different from those of vehicle-treated WT mice ($P = 0.15$). Repeated treatment with Cmpd-A did not statistically change the BDNF levels in the cortex of R6/2 mice ($P = 0.06$, Fig. 7B).

Cmpd-A Prevented Striatal Atrophy in R6/2 Mice.

Significant upregulation of BDNF levels in the striatum by Cmpd-A was expected to produce a neuroprotective effect against mutant huntingtin-induced neurodegeneration in R6/2 mice. Striatal atrophy in R6/2 mice was assessed by measuring striatal areas in the Nissl-stained brain sections of mice at 12 weeks of age (Fig. 8A). The area of the striatum was significantly reduced in brain sections from vehicle-treated R6/2 mice compared with those from vehicle-treated WT mice ($P \leq 0.01$; Fig. 8B). Repeated treatment with Cmpd-A at 5 mg/kg/day significantly inhibited the decline of striatal area in R6/2 mice ($P \leq 0.05$ at 5 mg/kg/day; Fig. 8B). This result suggests that Cmpd-A prevents striatal atrophy in R6/2 mice.

Cmpd-A Reduced Seizure Frequency but Did Not Prevent the Suppression of Body Weight Gain in R6/2 Mice.

I assessed effects of repeated treatment with Cmpd-A on general symptoms seen in R6/2 mice, including the suppression of body weight gain and increased susceptibility to seizures. The body weight of vehicle-treated WT mice increased gradually up to 11 weeks of age, whereas that of vehicle-treated R6/2 mice reached a plateau at 7 weeks of age (Fig. 9A). At 12 weeks of age, the body weight of vehicle-treated R6/2 mice was significantly lower than that of vehicle-treated WT mice ($P \leq 0.01$). Repeated treatment with Cmpd-A did not significantly prevent the suppression of body weight gain in R6/2 mice. Seizures were observed in R6/2

mice during the first 3 days of the acquisition phase when I tried to conduct water T-maze test at 9 weeks of age. These seizures were probably caused by water-immersion stress because R6/2 mice are known to have increased susceptibility to seizures triggered by stress (Mangiarini *et al.*, 1996). Repeated treatment of Cmpd-A dose-dependently and significantly suppressed seizure frequency in R6/2 mice ($P \leq 0.05$ at 5 mg/kg/day; Fig. 9B).

Cmpd-A Prevented Motor Deficits in R6/2 Mice.

To evaluate the effects of Cmpd-A on motor functions in R6/2 mice, I assessed the development of a clasping behavior and performed open field test and rotarod test. The foot clasping, an abnormal posturing of the hind limb during the tail suspension (Nguyen *et al.*, 2005), is a cardinal phenotype in R6/2 mice (Mangiarini *et al.*, 1996). I assessed foot clasping behavior weekly from 5 to 12 weeks of age. Vehicle-treated R6/2 mice, but not WT mice, exhibited clasping behavior after 8 weeks of age (Fig. 10A). Cmpd-A at 5 mg/kg/day tended to decrease the percentage of mice exhibiting clasping behavior at 10 and 11 weeks of age ($P = 0.07$ and 0.10, respectively), although the difference did not reach statistical significance (Fig. 10A). In open field test, vehicle-treated R6/2 mice showed significant decreases of total distance traveled and rearing frequency compared with vehicle-treated WT mice at 12 weeks of age (Fig. 10B and 10C). Repeated treatment with Cmpd-A dose-dependently inhibited the decrease of total distance traveled and rearing frequency ($P \leq 0.05$ at 5 mg/kg/day; Fig. 10B

and 9C). In rotarod test, R6/2 mice exhibited decrease of latency to fall off from the rotarod at 6 and 12 weeks of age, indicating the deficit in motor coordination (Fig. 10D). RM-ANOVA between WT and vehicle-treated R6/2 mice at each week of age showed significant effects of genotype at 6 and 12 weeks of age ($P \leq 0.01$). Repeated treatment with Cmpd-A did not prevent this deficit under these experimental conditions (Fig. 10D). These results suggest that in R6/2 mice, Cmpd-A prevents the deficits in motor functions, including the development of clasping behavior and the decreased activities in open field, but not the deficits in motor coordination on rotarod.

Cmpd-A Prevented Procedural Learning Deficits in Procedural Water T-Maze Test in R6/2 Mice.

To assess the efficacy of Cmpd-A for cognitive impairments in R6/2 mice, I conducted procedural water T-maze test at 9 to 10 weeks of age. In this test, procedural learning and cognitive flexibility can be evaluated in the acquisition and reversal phase, respectively (Tanimura *et al.*, 2008). This task is especially useful in assessing cognitive function in animals with motor impairments since the accuracy of their "choices" can be measured independently of their latency of escape, which may be perturbed by poor swimming performance (Melief *et al.*, 2015). Vehicle-treated R6/2 mice needed more days to reach the criteria than vehicle-treated WT mice in the acquisition phase, indicating impaired procedural

learning in R6/2 mice ($P \leq 0.01$; Fig. 11A). Repeated treatment with Cmpd-A dose-dependently and significantly reduced the numbers of days required to meet the criteria in R6/2 mice, suggesting the partial improvement in procedural learning by a high dose of Cmpd-A ($P \leq 0.05$ at 5 mg/kg/day; Fig. 11A).

Once the criteria were achieved within 7 days, the animals progressed to the reversal phase on an individual basis to characterize their cognitive flexibility. Eleven mice in each R6/2 mice group did not reach the criteria even after 7 days of acquisition phase and therefore were not evaluated in the reversal phase. On day 1 in the reversal phase, starting performance was different between groups. To assess the improvement in performance during the reversal phase, correct choice percentages on the latter half of this phase (days 4 to 6) were averaged and normalized by those on day 1. These values were represented as normalized correct choice percentages. The normalized correct choice percentages were significantly lower in R6/2 mice than WT mice in the reversal phase, suggesting impaired cognitive flexibility in R6/2 mice ($P \leq 0.05$; Fig. 11B). Repeated administration of Cmpd-A tended to increase the normalized correct choice percentages, although the effect did not reach statistical significance ($P = 0.09$ at 5 mg/kg/day; Fig. 11B). These results suggest that the high dose of Cmpd-A (5 mg/kg/day) partially prevents procedural learning deficits, whereas it does not have significant effects on the impairments of cognitive flexibility in R6/2 mice.

Cmpd-A Did Not Prevent Contextual Memory Deficits in CFC Test in R6/2 Mice.

To evaluate effects of Cmpd-A on contextual memory deficits in R6/2 mice, I conducted CFC test at 11 weeks of age. At the contextual phase 24 h after conditioning session, freezing behavior was significantly decreased in vehicle-treated R6/2 mice compared with vehicle-treated WT mice, indicating severe impairment of associative learning in R6/2 mice ($P \leq 0.01$; Fig. 12). Repeated administration of Cmpd-A did not increase the freezing time in R6/2 mice at the contextual phase. This result suggests that Cmpd-A does not prevent contextual memory deficits in R6/2 mice at 11 weeks of age.

Discussion

Indirect pathway MSNs appear to be more vulnerable than direct pathway MSNs in patients with HD (Galvan *et al.*, 2012). These differences in MSN vulnerability may provide unique opportunities in the future treatment of HD. Compared with other PDE10A inhibitors such as MP-10 and compound 1, Cmpd-A with a faster off-rate property activates the indirect pathway MSNs to a similar extent, whereas it partially activates the direct pathway MSNs (Suzuki *et al.*, 2016). This activation pattern of MSNs by Cmpd-A may protect MSNs in both pathways from neurotoxic effects of mutant huntingtin without inducing unbalanced activation of these neural pathways. I evaluated the effects of Cmpd-A on striatal neurodegeneration and behavioral deficits in the R6/2 mouse model of HD. The results were summarized and compared with the reported effects of TP-10 (Table 4).

BDNF plays a critical role in activity and survival of MSNs (Choi *et al.*, 2009). Striatal BDNF levels were decreased in R6/2 mice, and repeated treatment with Cmpd-A at 5 mg/kg/day almost completely prevented this reduction of BDNF levels at 12 weeks of age. Moreover, Cmpd-A at 5 mg/kg/day significantly prevented striatal atrophy in R6/2 mice at this age. These results suggest that the indirect pathway MSN-biased activation pattern by Cmpd-A is neuroprotective in the striatum of R6/2 mice. In addition, administration of Cmpd-A prevented the development of clasping behavior and deficits in motor functions in the open field, suggesting the prevention of disease progression in R6/2 mice. Cmpd-A did

not prevent the progressive deficit in motor coordination in rotarod test under these experimental conditions. Further studies would be needed but the impairment of motor coordination may be due to some functional deficits of the surviving MSNs, other brain regions, or peripheral regions.

The striatum and cortex are highly connected via neural circuitry (Haber, 2003; Simpson *et al.*, 2010), and this connectivity of the corticostriatal circuit enables sensory inputs to be associated with the output functions such as motor and cognitive responses, including procedural learning and cognitive flexibility (Tanimura *et al.*, 2008). Pharmacological magnetic resonance imaging and electroencephalography studies suggest that Cmpd-A likely modulates cortical activity through cortical-striatal-thalamic circuits (Tomimatsu *et al.*, 2016). Cmpd-A at 0.3 mg/kg improved cognitive functions in several rodent models (Shiraishi *et al.*, 2016). Therefore, in addition to neuroprotective effects of Cmpd-A, modulation of cortical functions through the corticostriatal circuit may also contribute to the improvement of cognitive function of R6/2 mice in the procedural water T-maze test. Cmpd-A did not prevent the deficit in contextual memory in R6/2 mice in CFC test at 11 weeks of age. The hippocampus plays an important role in the formation of contextual memory (Ramirez *et al.*, 2013). Autoradiography study using rat brain sections suggests that the PDE10A expression level in the hippocampus is quite low: 40-fold lower levels than that in the striatum (Harada *et al.*, 2015a). In addition, acute treatment with Cmpd-A did not increase cAMP and pCREB

levels in the mouse hippocampus (Suzuki *et al.*, 2015). Thus, Cmpd-A does not show significant improvement in contextual memory deficits in CFC test in R6/2 mice.

R6/2 mice are known to develop a tremor that worsens under stress and increases susceptibility to seizures (Cepeda-Prado *et al.*, 2012; Mangiarini *et al.*, 1996). The seizures observed in R6/2 mice during the procedural water T-maze test were probably triggered by the stress of water immersion. Intriguingly, Cmpd-A dose-dependently decreased seizure frequency. HD patients with more than 60 CAG repeats are afflicted by early and more aggressive pathologies, including myoclonic seizures, which are refractory to standard antiepileptic medications (Naydenov *et al.*, 2014). Cmpd-A could also have a potential therapeutic effect on myoclonic seizures in severe HD patients.

Cmpd-A did not prevent the suppression of body weight gain in R6/2 mice. TP-10 also showed no effects on it in R6/2 mice (Giampà *et al.*, 2010). Although the underlying mechanism of the suppression of body weight gain in mouse models of HD and in patients with HD remains unclear, peripheral effects of mutant huntingtin including wasting of skeletal muscle and adipose tissue are hypothesized (van der Burg *et al.*, 2009). PDE10A is selectively expressed in MSNs of the striatum; thus, if the suppression of body weight gain were due to peripheral effects of mutant huntingtin it would be reasonable that selective inhibition of PDE10A would have low impact on the suppression of body weight gain by mutant huntingtin in R6/2 mice.

Cmpd-A did not prevent the progressive deficit in motor coordination in a rotarod test under the present experimental conditions, whereas TP-10 was reported to significantly prevent the decline in rotarod performance in R6/2 mice (Giampà *et al.*, 2010). Although the precise reasons for this discrepancy remain unclear, differences in experimental conditions could possibly influence the pharmacological effects of the two compounds: animal husbandry and the acceleration and the maximum speed of rotarod are not consistent with those in TP-10 study. In line with this speculation, coenzyme Q10 and minocycline, potential drug candidates for the treatment of HD, produced conflicting results regarding their efficacy in rotarod test in R6/2 mice at least partially due to animal husbandry and testing protocols (Menalled *et al.*, 2010). To further investigate the differences of effects on impairment in motor coordination between Cmpd-A and TP-10, a direct comparison study under same experimental conditions is needed.

Some current antipsychotics with dopamine D_2 receptor antagonistic activity such as haloperidol and fluphenazine are commonly used to suppress chorea in HD by reducing involuntary movements through the activation of the indirect pathway (Bonelli and Wenning, 2006; Giménez-Roldán and Mateo, 1989). PDE10A inhibitors would also be expected to suppress chorea via PDE10A inhibition in the indirect pathway. However, PDE10A inhibitors activate both direct and indirect MSN pathways, and these pathways are considered to have competing effects on motor functions. In fact, a cataleptic response induced by activation of

the indirect pathway by haloperidol was canceled by excessive activation of the direct pathway by a D_1 receptor agonist SKF82958 in rats (Suzuki *et al.*, 2015). Moreover, several reports have suggested that excessive activation of the direct pathway MSNs is involved in the production of dystonia, one of the major clinical features of HD (Burbaud, 2012; Janavs and Aminoff, 1998; Louis *et al.*, 1999). It is not known whether the indirect pathway MSN-biased activation pattern by Cmpd-A would translate to therapeutic benefit in humans. Further preclinical and clinical studies are worth conducting to investigate pharmacological and tolerability profiles of Cmpd-A.

In this study, I used R6/2 mouse, a fragment Tg model, to evaluate the potential of Cmpd-A on HD. The R6/2 mouse is a widely used mouse model of HD for a preclinical study, because this fragment Tg model has a robust phenotype with an early onset, rapidly progressive neurodegeneration, weight loss, and motor and cognitive deficits (Pouladi *et al.*, 2013). However, there are also some caveats to the use of fragment Tg models to determine the preclinical efficacy of potential therapeutic candidates: widespread and relatively nonselective neuropathology, and/or a too rapid disease progression which may reduce the ability to detect the efficacy of a test compound (William Yang and Gray, 2011). Knock-in mouse models, such as CAG140, are thought to possess better face and construct validity compared with fragment Tg models because knock-in mouse models have a slow progression of phenotype, have a similar neuropathology to that of HD, and are genetically more representative of the

human disease under the endogenous huntingtin promoter (Ferrante, 2009; Menalled *et al.*, 2003). Thus, knock-in mouse models are considered to be a more faithful genetic model of the human condition. Although a pharmacological evaluation using knock-in mouse models with a slower phenotype progression will require longer study periods than fragment Tg models, further study using knock-in mouse models may provide additional information about the therapeutic potential of Cmpd-A in HD.

In summary, these results suggest that Cmpd-A with the indirect pathway MSN-biased activation pattern protects striatal neurons from degeneration and ameliorates behavioral deficits in the R6/2 mouse model of HD.

General Discussion

In HD, striatal MSNs are known to be the most vulnerable to the neurodegeneration (Vonsattel and DiFiglia, 1998). MSNs constitute two distinct output pathways from the striatum: the direct pathway projecting to SN, and the indirect pathway projecting to GP (Graybiel, 1990, 2000), and both MSNs undergo neurodegeneration in HD (Vonsattel and DiFiglia, 1998). Impairment in cAMP-CREB signaling pathway caused by mHTT aggregates has been hypothesized to play a critical role in HD pathology (Choi *et al.*, 2009; Gines *et al.*, 2003; Mantamadiotis *et al.*, 2002; Nucifora *et al.*, 2001; Sugars and Rubinsztein, 2003; Wyttenbach *et al.*, 2001). PDE10A is selectively expressed in both direct and indirect pathway MSNs and degrades cAMP (Bender and Beavo, 2006; Coskran *et al.*, 2006; Fujishige *et al.*, 1999; Seeger *et al.*, 2003). Thus, PDE10A inhibition would be a promising strategy to treat HD symptoms. To test this hypothesis, I obtained Cmpd-A, a tool inhibitor specific for PDE10A under physiological condition (part 1), and evaluated effects of PDE10A-specific inhibition on various phenotypes in HD model R6/2 mice using Cmpd-A (part 2).

Cmpd-A was identified as a potent and specific inhibitor for hPDE10A *in vitro*. Binding and functional activities of compounds for recombinant proteins are potentially different from those for proteins under physiological conditions due to differences in protein folding and/or binding partners. Therefore, I also checked binding activity and selectivity of Cmpd-A for naive PDE10A in rodents. By using *in vitro* ARG technique, I confirmed high binding affinity and high selectivity of Cmpd-A for native PDE10A protein of rats. *In vivo* ARG study using

rats also showed that orally administered Cmpd-A can readily penetrate into the brain and selectively bind to PDE10A protein *in vivo*. Here, I confirmed that Cmpd-A is an ideal tool to evaluate biological effects of PDE10A-specific inhibition under physiological conditions.

Although both MSNs undergo degeneration in HD, particularly indirect pathway MSNs are known to be more vulnerable to degeneration compared to direct pathway MSNs (Galvan *et al.*, 2012; Glass *et al.*, 2000; Reiner *et al.*, 1988; Sapp *et al.*, 1995). Given that overactivation of the direct pathway is suggested to be involved in the production of dystonia, one of the major clinical features of HD (Burbaud, 2012; Janavs and Aminoff, 1998; Louis *et al.*, 1999), activation of both MSNs without excessive activation of direct pathway MSNs seems to be beneficial for the treatment of HD symptoms. Dopamine D_1 receptor, predominantly expressed in direct pathway MSNs, is a G protein-coupled receptor (GPCR) coupled with G_s protein and increases cAMP when activated, while D_2 receptor, predominantly expressed in indirect pathway MSNs, is a GPCR coupled with G_i protein and decreases cAMP when stimulated (Missale *et al.*, 1998; Neve *et al.*, 2004). Therefore, cAMP concentration in direct pathway MSNs may be higher than that in indirect pathway MSNs under the basal conditions. Indeed, previous immunohistochemical study showed that more than 90% of cAMP-positive cells were substance P (a marker of direct pathway MSNs)-positive in the rat striatum (Suzuki *et al.*, 2016). Enzyme substrates are degraded at the binding pockets in the catalytic domains of enzymes. Competitive enzyme inhibitors prevent substrate degradation by binding

competition with the substrates at the binding pockets. Thus, inhibitory effects of competitive enzyme inhibitors depend on concentrations of substrates and inhibitors, and dissociation rates (off-rates) of inhibitors. In general, competitive enzyme inhibitors with faster off-rates are more sensitive to binding competition with the enzyme substrates compared to inhibitors with slower off-rate especially at higher concentrations of substrates. In the case of PDE10A inhibitors, compared with slower off-rate ones, faster off-rate ones may inhibit PDE10A equally in indirect pathway MSNs but more weakly in direct pathway MSNs due to the higher cAMP levels in direct pathway MSNs than indirect pathway MSNs. *In vitro* ARG study using rat brain slices revealed that Cmpd-A dissociated from PDE10A clearly faster than MP-10 (Suzuki *et al.*, 2016). Moreover, analysis of pathway-specific markers showed that compared with MP-10, Cmpd-A equally activated indirect pathway MSNs, while it partially activated direct pathway MSNs (Suzuki *et al.*, 2016). Thus, Cmpd-A could be an ideal tool to produce a balanced activation of both MSNs without excess activation of direct pathway MSNs (indirect pathway MSN-biased activation) by specific and unique PDE10A inhibition *in vivo*.

To examine the therapeutic potential of the balanced activation of both direct and indirect pathway MSNs based on specific and unique PDE10A inhibition for the treatment of HD, effects of repeated treatment with Cmpd-A on various phenotypes of HD model R6/2 mice were investigated. Compared to WT mice, R6/2 mice showed reduced BDNF levels in the striatum, reduction of striatal areas, higher frequency of stress (water immersion)-induced

seizures, lower body weight. Regarding motor functions, R6/2 mice exhibited progressive clasping behavior, decline of locomotor activity in the open field, deficits in motor co-ordination in the rotarod test. As for cognitive functions, deficits in procedural learning and cognitive flexibility in the procedural water T-maze task, and a severe impairment of associative memory in the CFC test were observed in R6/2 mice. Repeated treatment with Cmpd-A dose-dependently prevented the reduction of striatal BDNF levels and striatal atrophy in R6/2 mice. Because BDNF is known to play a critical role in activity and survival of MSNs (Choi *et al.*, 2009; Zuccato and Cattaneo, 2007), prevention of decrease in striatal BDNF levels might contribute to the protection of MSNs from degeneration. Cmpd-A reduced the increased frequency of stress-induced seizures, and prevented the progression of several deficits such as development of clasping behavior and decline of locomotion, and improved the procedural learning impairment in R6/2 mice. These findings demonstrate that the balanced activation of both MSNs by specific and unique inhibition of PDE10A improves several phenotypes in R6/2 mice.

Recently, Pfizer announced that in a clinical study named 'Amaryllis' trial, PF-02545920 (MP-10) failed to improve HD symptoms (ClinicaTrials.gov Identifier: NCT02197130). It was also recently reported that MP-10 did not affect the worsened neurological index, but modestly improved striatal volume measured by *in vivo* MRI and some motor deficits in Q175 knock-in mouse model for HD (Beaumont *et al.*, 2016). As mentioned above, MP-10 has a

slower off-rate property and elicits excess activation of direct pathway MSNs compared to Cmpd-A. Although HD model animals available to date may not completely replicate the HD pathology, head-to-head comparison between Cmpd-A and MP-10 using these models will further provide some insight into the therapeutic potential of different modes of PDE10A inhibition for HD symptoms. Nevertheless, the current study suggests that the balanced activation of both direct and indirect pathway MSNs based on specific and unique inhibition of PDE10A has some potential to improve HD symptoms. Furthermore, the findings in the present study will help us better understand the biological function of PDE10A.

Acknowledgements

I am most grateful to Professor Kazuto Nakada, University of Tsukuba, for his continuous guidance and valuable discussions through my doctoral program. I am also grateful to Professor Tomoki Chiba, Professor Kenji Miura, and Associate Professor Hidekazu Kuwayama, University of Tsukuba, for their helpful discussion on my doctoral dissertation.

I wish to express our sincere thanks to Hirobumi Suzuki, Takeda Pharmaceutical Company Limited for experimental assistance, and to Noriyasu Sano, Takeda Pharmaceutical Company Limited for technical instruction of the PDE10A occupancy study. I also thank Jun Kunitomo, Takeda Pharmaceutical Company Limited for providing chemical compounds.

I thank PsychoGenics Inc. for conducting behavioral experiments, Drug Metabolism and Pharmacokinetics Research Laboratories, Takeda Pharmaceutical Company Limited for analysis of Cmpd-A exposure and PDE10A occupancy, and Motohisa Suzuki, Takeda Pharmaceutical Company Limited for the blind evaluation of histological data.

References

Akar, F., Mutlu, O., Celikyurt, I.K., Bektas, E., Tanyeri, M.H., *et al.* (2014). Effects of Zaprinast and Rolipram on Olfactory and Visual Memory in the Social Transmission of Food Preference and Novel Object Recognition Tests in Mice. Drug Target Insights *8*, 23-29.

Beaumont, V., Zhong, S., Lin, H., Xu, W., Bradaia, A., *et al.* (2016). Phosphodiesterase 10A Inhibition Improves Cortico-Basal Ganglia Function in Huntington's Disease Models. Neuron.

Bender, A.T., and Beavo, J.A. (2006). Cyclic nucleotide phosphodiesterases: molecular regulation to clinical use. Pharmacol Rev *58*, 488-520.

Bonelli, R.M., and Wenning, G.K. (2006). Pharmacological management of Huntington's disease: an evidence-based review. Curr Pharm Des *12*, 2701-2720.

Burbaud, P. (2012). Dystonia Pathophysiology: A Critical Review, in *Dystonia: The Many facets*, R. Rosales, ed. (InTech), pp. 199-220.

Cepeda-Prado, E., Popp, S., Khan, U., Stefanov, D., Rodriguez, J., *et al.* (2012). R6/2 Huntington's disease mice develop early and progressive abnormal brain metabolism and seizures. J Neurosci *32*, 6456-6467.

Chernet, E., Martin, L.J., Li, D., Need, A.B., Barth, V.N., *et al.* (2005). Use of LC/MS to assess brain tracer distribution in preclinical, in vivo receptor occupancy studies: dopamine D2, serotonin 2A and NK-1 receptors as examples. Life Sci *78*, 340-346.

Choi, Y.S., Lee, B., Cho, H.Y., Reyes, I.B., Pu, X.A., *et al.* (2009). CREB is a key regulator

of striatal vulnerability in chemical and genetic models of Huntington's disease. Neurobiol Dis *36*, 259-268.

Coskran, T.M., Morton, D., Menniti, F.S., Adamowicz, W.O., Kleiman, R.J., *et al.* (2006). Immunohistochemical localization of phosphodiesterase 10A in multiple mammalian species. J Histochem Cytochem *54*, 1205-1213.

Cote, R.H. (2004). Characteristics of photoreceptor PDE (PDE6): similarities and differences to PDE5. Int J Impot Res *16 Suppl 1*, S28-33.

Crook, Z.R., and Housman, D.E. (2012). Dysregulation of dopamine receptor D2 as a sensitive measure for Huntington disease pathology in model mice. Proc Natl Acad Sci U S A *109*, 7487-7492.

Ferrante, R.J. (2009). Mouse models of Huntington's disease and methodological considerations for therapeutic trials. Biochim Biophys Acta *1792*, 506-520.

Frank, S. (2014). Treatment of Huntington's disease. Neurotherapeutics *11*, 153-160.

Fujishige, K., Kotera, J., Michibata, H., Yuasa, K., Takebayashi, S., *et al.* (1999). Cloning and characterization of a novel human phosphodiesterase that hydrolyzes both cAMP and cGMP (PDE10A). J Biol Chem *274*, 18438-18445.

Galvan, L., Andre, V.M., Wang, E.A., Cepeda, C., and Levine, M.S. (2012). Functional Differences Between Direct and Indirect Striatal Output Pathways in Huntington's Disease. J Huntingtons Dis *1*, 17-25.

Giampà, C., Laurenti, D., Anzilotti, S., Bernardi, G., Menniti, F.S., and Fusco, F.R. (2010). Inhibition of the striatal specific phosphodiesterase PDE10A ameliorates striatal and cortical pathology in R6/2 mouse model of Huntington's disease. PLoS One *5*, e13417.

Giampà, C., Patassini, S., Borreca, A., Laurenti, D., Marullo, F., *et al.* (2009). Phosphodiesterase 10 inhibition reduces striatal excitotoxicity in the quinolinic acid model of Huntington's disease. Neurobiol Dis *34*, 450-456.

Giménez-Roldán, S., and Mateo, D. (1989). [Huntington disease: tetrabenazine compared to haloperidol in the reduction of involuntary movements]. Neurologia *4*, 282-287.

Gines, S., Seong, I.S., Fossale, E., Ivanova, E., Trettel, F., *et al.* (2003). Specific progressive cAMP reduction implicates energy deficit in presymptomatic Huntington's disease knock-in mice. Hum Mol Genet *12*, 497-508.

Glass, M., Dragunow, M., and Faull, R.L. (2000). The pattern of neurodegeneration in Huntington's disease: a comparative study of cannabinoid, dopamine, adenosine and GABA(A) receptor alterations in the human basal ganglia in Huntington's disease. Neuroscience *97*, 505-519.

Godinho, B.M., Malhotra, M., O'Driscoll, C.M., and Cryan, J.F. (2014). Delivering a disease-modifying treatment for Huntington's disease. Drug Discov Today.

Grauer, S.M., Pulito, V.L., Navarra, R.L., Kelly, M.P., Kelley, C., *et al.* (2009). Phosphodiesterase 10A inhibitor activity in preclinical models of the positive, cognitive, and

negative symptoms of schizophrenia. J Pharmacol Exp Ther *331*, 574-590.

Graybiel, A.M. (1990). Neurotransmitters and neuromodulators in the basal ganglia. Trends Neurosci *13*, 244-254.

Graybiel, A.M. (2000). The basal ganglia. Curr Biol *10*, R509-511.

Haber, S.N. (2003). The primate basal ganglia: parallel and integrative networks. J Chem Neuroanat *26*, 317-330.

Harada, A., Suzuki, K., Kamiguchi, N., Miyamoto, M., Tohyama, K., *et al.* (2015a). Characterization of Binding and Inhibitory Properties of TAK-063, a Novel Phosphodiesterase 10A Inhibitor. PLoS One *10*, e0122197.

Harada, A., Suzuki, K., Miura, S., Hasui, T., Kamiguchi, N., *et al.* (2015b). Characterization of the binding properties of T-773 as a PET radioligand for phosphodiesterase 10A. Nucl Med Biol *42*, 146-154.

Janavs, J.L., and Aminoff, M.J. (1998). Dystonia and chorea in acquired systemic disorders. J Neurol Neurosurg Psychiatry *65*, 436-445.

Karam, C.S., Ballon, J.S., Bivens, N.M., Freyberg, Z., Girgis, R.R., *et al.* (2010). Signaling pathways in schizophrenia: emerging targets and therapeutic strategies. Trends Pharmacol Sci *31*, 381-390.

Kehler, J., and Nielsen, J. (2011). PDE10A inhibitors: novel therapeutic drugs for schizophrenia. Curr Pharm Des *17*, 137-150.

Kleiman, R.J., Kimmel, L.H., Bove, S.E., Lanz, T.A., Harms, J.F., *et al.* (2011). Chronic suppression of phosphodiesterase 10A alters striatal expression of genes responsible for neurotransmitter synthesis, neurotransmission, and signaling pathways implicated in Huntington's disease. J Pharmacol Exp Ther *336*, 64-76.

Krebs, M., Leopold, K., Hinzpeter, A., and Schaefer, M. (2006). Current schizophrenia drugs: efficacy and side effects. Expert Opin Pharmacother *7*, 1005-1016.

Kunitomo, J., Yoshikawa, M., Fushimi, M., Kawada, A., Quinn, J.F., *et al.* (2014). Discovery of 1-[2-Fluoro-4-(1H-pyrazol-1-yl)phenyl]-5-methoxy-3-(1-phenyl-1H-pyrazol-5-yl)pyri dazin-4(1H)-one (TAK-063), a Highly Potent, Selective, and Orally Active Phosphodiesterase 10A (PDE10A) Inhibitor. J Med Chem *57*, 9627-9643.

Lüesse, H.G., Schiefer, J., Spruenken, A., Puls, C., Block, F., and Kosinski, C.M. (2001). Evaluation of R6/2 HD transgenic mice for therapeutic studies in Huntington's disease: behavioral testing and impact of diabetes mellitus. Behav Brain Res *126*, 185-195.

Lei, W., Jiao, Y., Del Mar, N., and Reiner, A. (2004). Evidence for differential cortical input to direct pathway versus indirect pathway striatal projection neurons in rats. J Neurosci *24*, 8289-8299.

Louis, E.D., Lee, P., Quinn, L., and Marder, K. (1999). Dystonia in Huntington's disease: Prevalence and clinical characteristics. Mov Disord *14*, 95-101.

Mangiarini, L., Sathasivam, K., Seller, M., Cozens, B., Harper, A., *et al.* (1996). Exon 1 of the HD gene with an expanded CAG repeat is sufficient to cause a progressive neurological phenotype in transgenic mice. Cell *87*, 493-506.

Mantamadiotis, T., Lemberger, T., Bleckmann, S.C., Kern, H., Kretz, O., *et al.* (2002). Disruption of CREB function in brain leads to neurodegeneration. Nat Genet *31*, 47-54.

Melief, E.J., Cudaback, E., Jorstad, N.L., Sherfield, E., Postupna, N., *et al.* (2015). Partial depletion of striatal dopamine enhances penetrance of cognitive deficits in a transgenic mouse model of Alzheimer's disease. J Neurosci Res *93*, 1413-1422.

Menalled, L.B., Kudwa, A.E., Oakeshott, S., Farrar, A., Paterson, N., *et al.* (2014). Genetic deletion of transglutaminase 2 does not rescue the phenotypic deficits observed in R6/2 and zQ175 mouse models of Huntington's disease. PLoS One *9*, e99520.

Menalled, L.B., Patry, M., Ragland, N., Lowden, P.A., Goodman, J., *et al.* (2010). Comprehensive behavioral testing in the R6/2 mouse model of Huntington's disease shows no benefit from CoQ10 or minocycline. PLoS One *5*, e9793.

Menalled, L.B., Sison, J.D., Dragatsis, I., Zeitlin, S., and Chesselet, M.F. (2003). Time course of early motor and neuropathological anomalies in a knock-in mouse model of Huntington's disease with 140 CAG repeats. J Comp Neurol *465*, 11-26.

Menniti, F.S., Chappie, T.A., Humphrey, J.M., and Schmidt, C.J. (2007). Phosphodiesterase 10A inhibitors: a novel approach to the treatment of the symptoms of

schizophrenia. Curr Opin Investig Drugs *8*, 54-59.

Missale, C., Nash, S.R., Robinson, S.W., Jaber, M., and Caron, M.G. (1998). Dopamine receptors: from structure to function. Physiol Rev *78*, 189-225.

Mori, F., Pérez-Torres, S., De Caro, R., Porzionato, A., Macchi, V., *et al.* (2010). The human area postrema and other nuclei related to the emetic reflex express cAMP phosphodiesterases 4B and 4D. J Chem Neuroanat *40*, 36-42.

Naydenov, A.V., Horne, E.A., Cheah, C.S., Swinney, K., Hsu, K.L., *et al.* (2014). ABHD6 blockade exerts antiepileptic activity in PTZ-induced seizures and in spontaneous seizures in R6/2 mice. Neuron *83*, 361-371.

Neve, K.A., Seamans, J.K., and Trantham-Davidson, H. (2004). Dopamine receptor signaling. J Recept Signal Transduct Res *24*, 165-205.

Nguyen, T., Hamby, A., and Massa, S.M. (2005). Clioquinol down-regulates mutant huntingtin expression in vitro and mitigates pathology in a Huntington's disease mouse model. Proc Natl Acad Sci U S A *102*, 11840-11845.

Nirogi, R., Kandikere, V., Bhyrapuneni, G., Muddana, N., Saralaya, R., *et al.* (2012). In vivo receptor occupancy assay of histamine H(3) receptor antagonist in rats using non-radiolabeled tracer. J Pharmacol Toxicol Methods *65*, 115-121.

Nishi, A., Kuroiwa, M., Miller, D.B., O'Callaghan, J.P., Bateup, H.S., *et al.* (2008). Distinct roles of PDE4 and PDE10A in the regulation of cAMP/PKA signaling in the striatum.

J Neurosci *28*, 10460-10471.

Norris, P.J., Waldvogel, H.J., Faull, R.L., Love, D.R., and Emson, P.C. (1996). Decreased neuronal nitric oxide synthase messenger RNA and somatostatin messenger RNA in the striatum of Huntington's disease. Neuroscience *72*, 1037-1047.

Nucifora, F.C., Jr., Sasaki, M., Peters, M.F., Huang, H., Cooper, J.K., *et al.* (2001). Interference by huntingtin and atrophin-1 with cbp-mediated transcription leading to cellular toxicity. Science *291*, 2423-2428.

Padovan-Neto, F.E., Sammut, S., Chakroborty, S., Dec, A.M., Threlfell, S., *et al.* (2015). Facilitation of corticostriatal transmission following pharmacological inhibition of striatal phosphodiesterase 10A: role of nitric oxide-soluble guanylyl cyclase-cGMP signaling pathways. J Neurosci *35*, 5781-5791.

Paxinos, G., and Franklin, K.B.J. (2001). The mouse brain in stereotaxic coordinates., 2nd edn (San Diego: Academic Press).

Paxinos, G., and Watson, C. (1998). The rat brain in stereotaxic coordinates., 4th edn (San Diego: Academic Press).

Pouladi, M.A., Morton, A.J., and Hayden, M.R. (2013). Choosing an animal model for the study of Huntington's disease. Nat Rev Neurosci *14*, 708-721.

Ramirez, S., Tonegawa, S., and Liu, X. (2013). Identification and optogenetic manipulation of memory engrams in the hippocampus. Front Behav Neurosci *7*, 226.

Reiner, A., Albin, R.L., Anderson, K.D., D'Amato, C.J., Penney, J.B., and Young, A.B. (1988). Differential loss of striatal projection neurons in Huntington disease. Proc Natl Acad Sci U S A *85*, 5733-5737.

Reinius, B., Blunder, M., Brett, F.M., Eriksson, A., Patra, K., *et al.* (2015). Conditional targeting of medium spiny neurons in the striatal matrix. Front Behav Neurosci *9*, 71.

Reneerkens, O.A., Rutten, K., Bollen, E., Hage, T., Blokland, A., *et al.* (2013). Inhibition of phoshodiesterase type 2 or type 10 reverses object memory deficits induced by scopolamine or MK-801. Behav Brain Res *236*, 16-22.

Ross, C.A., Aylward, E.H., Wild, E.J., Langbehn, D.R., Long, J.D., *et al.* (2014). Huntington disease: natural history, biomarkers and prospects for therapeutics. Nat Rev Neurol *10*, 204-216.

Ross, C.A., and Tabrizi, S.J. (2011). Huntington's disease: from molecular pathogenesis to clinical treatment. Lancet Neurol *10*, 83-98.

Rourke, C., Starr, K.R., Reavill, C., Fenwick, S., Deadman, K., and Jones, D.N. (2006). Effects of the atypical antipsychotics olanzapine and risperidone on plasma prolactin levels in male rats: a comparison with clinical data. Psychopharmacology (Berl) *184*, 107-114.

Sapp, E., Ge, P., Aizawa, H., Bird, E., Penney, J., *et al.* (1995). Evidence for a preferential loss of enkephalin immunoreactivity in the external globus pallidus in low grade Huntington's disease using high resolution image analysis. Neuroscience *64*, 397-404.

Scheuing, L., Chiu, C.T., Liao, H.M., Linares, G.R., and Chuang, D.M. (2014). Preclinical and clinical investigations of mood stabilizers for Huntington's disease: what have we learned? Int J Biol Sci *10*, 1024-1038.

Schmidt, C.J., Chapin, D.S., Cianfrogna, J., Corman, M.L., Hajos, M., *et al.* (2008). Preclinical characterization of selective phosphodiesterase 10A inhibitors: a new therapeutic approach to the treatment of schizophrenia. J Pharmacol Exp Ther *325*, 681-690.

Seeger, T.F., Bartlett, B., Coskran, T.M., Culp, J.S., James, L.C., *et al.* (2003). Immunohistochemical localization of PDE10A in the rat brain. Brain Res *985*, 113-126.

Shiraishi, E., Suzuki, K., Harada, A., Suzuki, N., and Kimura, H. (2016). The Phosphodiesterase 10A Selective Inhibitor TAK-063 Improves Cognitive Functions Associated with Schizophrenia in Rodent Models. J Pharmacol Exp Ther *356*, 587-595.

Shirley, E. (1977). A non-parametric equivalent of Williams' test for contrasting increasing dose levels of a treatment. Biometrics *33*, 386-389.

Simpson, E.H., Kellendonk, C., and Kandel, E. (2010). A possible role for the striatum in the pathogenesis of the cognitive symptoms of schizophrenia. Neuron *65*, 585-596.

Siuciak, J.A., Chapin, D.S., Harms, J.F., Lebel, L.A., McCarthy, S.A., *et al.* (2006). Inhibition of the striatum-enriched phosphodiesterase PDE10A: a novel approach to the treatment of psychosis. Neuropharmacology *51*, 386-396.

Slow, E.J., van Raamsdonk, J., Rogers, D., Coleman, S.H., Graham, R.K., *et al.* (2003).

Selective striatal neuronal loss in a YAC128 mouse model of Huntington disease. Hum Mol Genet *12*, 1555-1567.

Soderling, S.H., Bayuga, S.J., and Beavo, J.A. (1999). Isolation and characterization of a dual-substrate phosphodiesterase gene family: PDE10A. Proc Natl Acad Sci U S A *96*, 7071-7076.

Sugars, K.L., and Rubinsztein, D.C. (2003). Transcriptional abnormalities in Huntington disease. Trends Genet *19*, 233-238.

Suzuki, K., Harada, A., Shiraishi, E., and Kimura, H. (2015). In Vivo Pharmacological Characterization of TAK-063, a Potent and Selective Phosphodiesterase 10A Inhibitor with Antipsychotic-Like Activity in Rodents. J Pharmacol Exp Ther *352*, 471-479.

Suzuki, K., Harada, A., Suzuki, H., Miyamoto, M., and Kimura, H. (2016). TAK-063, a PDE10A Inhibitor with Balanced Activation of Direct and Indirect Pathways, Provides Potent Antipsychotic-Like Effects in Multiple Paradigms. Neuropsychopharmacology *41*, 2252-2262.

Tanimura, Y., Yang, M.C., and Lewis, M.H. (2008). Procedural learning and cognitive flexibility in a mouse model of restricted, repetitive behaviour. Behav Brain Res *189*, 250-256.

Tardito, D., Perez, J., Tiraboschi, E., Musazzi, L., Racagni, G., and Popoli, M. (2006). Signaling pathways regulating gene expression, neuroplasticity, and neurotrophic mechanisms

in the action of antidepressants: a critical overview. Pharmacol Rev *58*, 115-134.

Thakur, T., Sharma, S., Kumar, K., Deshmukh, R., and Sharma, P.L. (2013). Neuroprotective role of PDE4 and PDE5 inhibitors in 3-nitropropionic acid induced behavioral and biochemical toxicities in rats. Eur J Pharmacol *714*, 515-521.

Threlfell, S., Sammut, S., Menniti, F.S., Schmidt, C.J., and West, A.R. (2009). Inhibition of Phosphodiesterase 10A Increases the Responsiveness of Striatal Projection Neurons to Cortical Stimulation. J Pharmacol Exp Ther *328*, 785-795.

Tomimatsu, Y., Cash, D., Suzuki, M., Suzuki, K., Bernanos, M., *et al.* (2016). TAK-063, a phosphodiesterase 10A inhibitor, modulates neuronal activity in various brain regions in phMRI and EEG studies with and without ketamine challenge. Neuroscience *339*, 180-190.

van der Burg, J.M., Bjorkqvist, M., and Brundin, P. (2009). Beyond the brain: widespread pathology in Huntington's disease. Lancet Neurol *8*, 765-774.

Verhoest, P.R., Chapin, D.S., Corman, M., Fonseca, K., Harms, J.F., *et al.* (2009). Discovery of a novel class of phosphodiesterase 10A inhibitors and identification of clinical candidate 2-[4-(1-methyl-4-pyridin-4-yl-1H-pyrazol-3-yl)-phenoxymethyl]-quinoline (PF-2545920) for the treatment of schizophrenia. J Med Chem *52*, 5188-5196.

Vonsattel, J.P., and DiFiglia, M. (1998). Huntington disease. J Neuropathol Exp Neurol *57*, 369-384.

Walker, F.O. (2007). Huntington's disease. The Lancet *369*, 218-228.

William Yang, X., and Gray, M. (2011). Mouse Models for Validating Preclinical Candidates for Huntington's Disease, in *Neurobiology of Huntington's Disease: Applications to Drug Discovery*, D.C. Lo, and R.E. Hughes, eds. (Boca Raton (FL): CRC Press/Taylor & Francis Llc.).

Williams, D.A. (1971). A test for differences between treatment means when several dose levels are compared with a zero dose control. Biometrics *27*, 103-117.

Wilson, J.M., Ogden, A.M., Loomis, S., Gilmour, G., Baucum, A.J., 2nd, *et al.* (2015). Phosphodiesterase 10A inhibitor, MP-10 (PF-2545920), produces greater induction of c-Fos in dopamine D2 neurons than in D1 neurons in the neostriatum. Neuropharmacology *99*, 379-386.

Wyttenbach, A., Swartz, J., Kita, H., Thykjaer, T., Carmichael, J., *et al.* (2001). Polyglutamine expansions cause decreased CRE-mediated transcription and early gene expression changes prior to cell death in an inducible cell model of Huntington's disease. Hum Mol Genet *10*, 1829-1845.

Zuccato, C., and Cattaneo, E. (2007). Role of brain-derived neurotrophic factor in Huntington's disease. Prog Neurobiol *81*, 294-330.

Tables

Table 1. Percent inhibition of enzymes by Cmpd-A at 10 µM.

Enzyme	**% inhibition**
Acetylcholinesterase	3
ATPase, Ca„$^{2+}$, Skeletal Muscle	6
ATPase, Na^{+}/K^{+}, Heart	8
Carbonic anhydrase II	6
Cyclooxygenase-1 (COX-1)	26
Cyclooxygenase-2 (COX-2)	6
EGF receptor tyrosine kinase	5
HMG-CoA reductase	11
5-Lipoxygenase (5-LO)	3
Monoamine oxidase A (MAO-A)	16
Monoamine oxidase B (MAO-B)	10
Nitric oxide synthase, inducible (iNOS)	1
Nitric oxide synthase, neuronal (nNOS)	12
Peptidase, factor Xa	1
Matrix metalloproteinase-1 (MMP-1)	9
Matrix metalloproteinase-7 (MMP-7)	7
Matrix metalloproteinase-13 (MMP-13)	11

Phosphodiesterase PDE3	23
Phosphodiesterase PDE4	50
Phosphodiesterase PDE5	44
Phosphodiesterase PDE6	20
Phosphodiesterase PDE10A1	101
Protein kinase A (PKA), nonselective	−3
Protein kinase C (PKC), nonselective	7
Steroid 5α-reductase	16
Xanthine oxidase	−3

EGF, epidermal growth factor; HMG CoA, 3-hydroxy-3-methyl-glutaryl coenzyme A.

Negative value of percent inhibition indicates activation of enzyme activity.

Table 2. Percent inhibition of receptors by Cmpd-A at 10 µM.

Receptor	**% inhibition**
Adenosine A_1	11
Adenosine A_{2A}	−4
Adenosine A_{2B}	0
Adrenergic α_1, non-selective	14
Adrenergic α_2, non-selective	−2
Adrenergic β_1	6
Adrenergic β_2	6
Adrenergic β_3	1
Androgen (testosterone)	6
Angiotensin AT_1	13
Angiotensin AT_2	−4
Bradykinin B_1	11
Bradykinin B_2	−2
Calcium channel L-type, benzothiazepine	3
Calcium channel L-type, dihydropyridine	0
Calcium channel L-type, phenylalkylamine	4
Calcium channel N-type	−3

Cannabinoid CB_1	3
Cholecystokinin CCK_1 (CCK_A)	5
Cholecystokinin CCK_2 (CCK_B)	1
Dopamine D_1	8
Dopamine D_{2L}	−7
Dopamine D_3	−1
Dopamine $D_{4.2}$	7
Dopamine transporter (DAT)	11
Estrogen ERα	3
$GABA_A$, chloride channel	12
$GABA_A$, flunitrazepam, central	−3
$GABA_A$, muscimol, central	0
$GABA_A$, non-selective	7
$GABA_{B1A}$	−18
$GABA_{B1B}$	−13
GABA transporter	11
Glucocorticoid	−5
Glutamate, AMPA	−6
Glutamate, kainate	5

Glutamate, NMDA	24
Glutamate, NMDA, glycine	11
Glutamate, NMDA, phencyclidine	0
Glycine, strychninee	−1
Growth hormone secretagogue (ghrelin)	1
Histamine H_1	−8
Histamine H_2	−5
Imidazoline I_2, central	7
Insulin	−8
Muscarinic M_1	4
Muscarinic M_2	−10
Muscarinic M_3	−1
Nicotinic acetylcholine	1
Norepinephrine transporter (NET)	15
Opiate δ (OP1, DOP)	16
Opiate κ (OP2, KOP)	5
Opiate μ (OP3, MOP)	−1
Potassium channel (K_{ATP})	12
Potassium channel (SK_{CA})	5

Progesterone PR-B	0
Prostanoid / thromboxane A_2 (TP)	13
Serotonin 5-HT_1, non-selective	15
Serotonin 5-HT_2, non-selective	23
Serotonin 5-HT_{2B}	14
Serotonin 5-HT_3	−3
Serotonin 5-HT_4	−1
Serotonin transporter (SERT)	−5
Sigma, non-selective	−9
Sodium channel, Site 2	15
Tachykinin NK_1	−2
Tachykinin NK_2	0
Tachykinin NK_3	−11
Vasopressin V_{1A}	4
Vasopressin V_2	−2

AMPA, α-amino-3-hydroxy-5-methyl-4-isoxazolepropionic acid; NMDA, N-methyl-$_D$-aspartic acid. Negative value of percent inhibition indicates stimulation of receptor activity.

Table 3. Concentration of T-773 in the rat brain and displacement by Cmpd-A.

	Dose of Cmpd-A (mg/kg, p.o.)						
Brain area	**0**	**0.03**	**0.1**	**0.3**	**1**	**3**	**10**
Striatum	26.1 ± 2.6	28.5 ± 2.0	22.2 ± 0.9	15.9	12.9 ± 0.9	8.9 ± 0.4	5.3 ± 0.4
Cerebellum	5.0 ± 0.4	4.4 ± 0.4	3.6 ± 0.2	2.8	3.2 ± 0.4	2.8 ± 0.1	2.9 ± 0.6

The data (ng/g tissue) are represented as mean (n=2 at 0.3 mg/kg) or mean ± SEM (n=3).

Table 4. Comparison of the effects on the phenotypes of R6/2 mice between Cmpd-A and TP-10.

		Effect of test compound	
		Cmpd-A	TP-10
Neural protection and brain pathology	Reduction of BDNF levels	Suppression (striatum)	Suppression (striatum and cortex)
	Striatal atrophy	Prevention	Prevention
	Formation of NIIs	NT	Reduction
	Microglial activation	NT	Inhibition
General behavior	Loss of righting reflex (survival)	NT	Inhibition
	Suppression of body weight gain	No effect	No effect
	Increase in seizure frequency	Suppression	NT
Motor function	Development of a clasping behavior	Prevention	Prevention
	Decrease in motor activity (open field test)	Inhibition	Inhibition
	Deficit in motor coordination	No effect	Improvement

	(rotarod test)		
Cognitive function	Deficits in procedural learning and cognitive flexibility (water T-maze test)	Improvement (procedural learning)	NT
	Deficit in contextual memory (contextual fear conditioning test)	No effect	NT

The results of TP-10 are reported by Giampà *et al*. (2010).

BDNF, brain-derived neurotrophic factor; NIIs, neuronal intranuclear inclusions; NT, not tested.

Figures

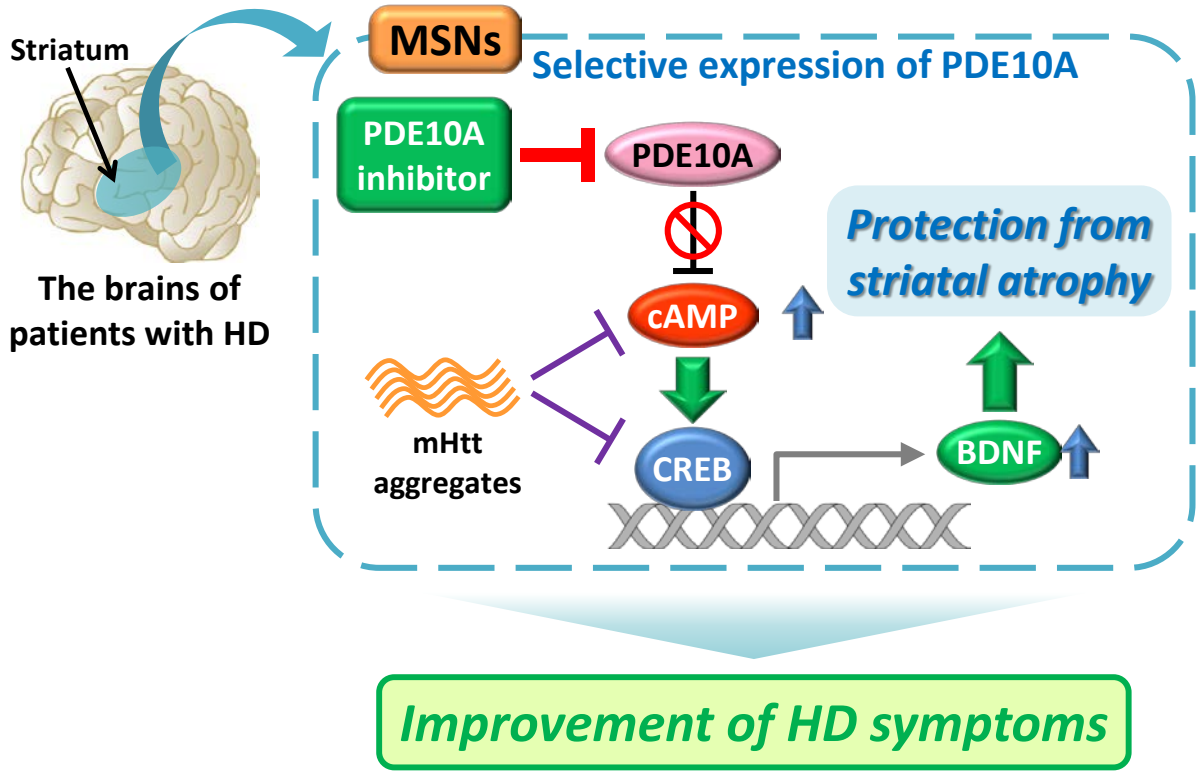

Figure 1. Schematic illustration of the therapeutic strategy for Huntington's disease (HD) by phosphodiesterase 10A (PDE10A) inhibition. In striatal medium spiny neurons (MSNs) of patients with HD, cyclic adenosine monophosphate (cAMP)-cAMP response element-binding protein (CREB) signaling could be impaired by mutant Huntingtin (mHtt) aggregates. This has been hypothesized to play a critical role in HD pathology. PDE10A is selectively expressed in mammalian MSNs and degrades cAMP, thus PDE10A inhibition can enhance cAMP-CREB signaling selectively in MSNs. Therefore, PDE10A inhibition could be a promising therapeutic strategy for HD. Here, I demonstrate that specific inhibition of PDE10A by Cmpd-A suppresses reduction of striatal brain-derived neurotrophic factor (BDNF), prevents striatal atrophy, and improves several phenotypes in HD model R6/2 mice.

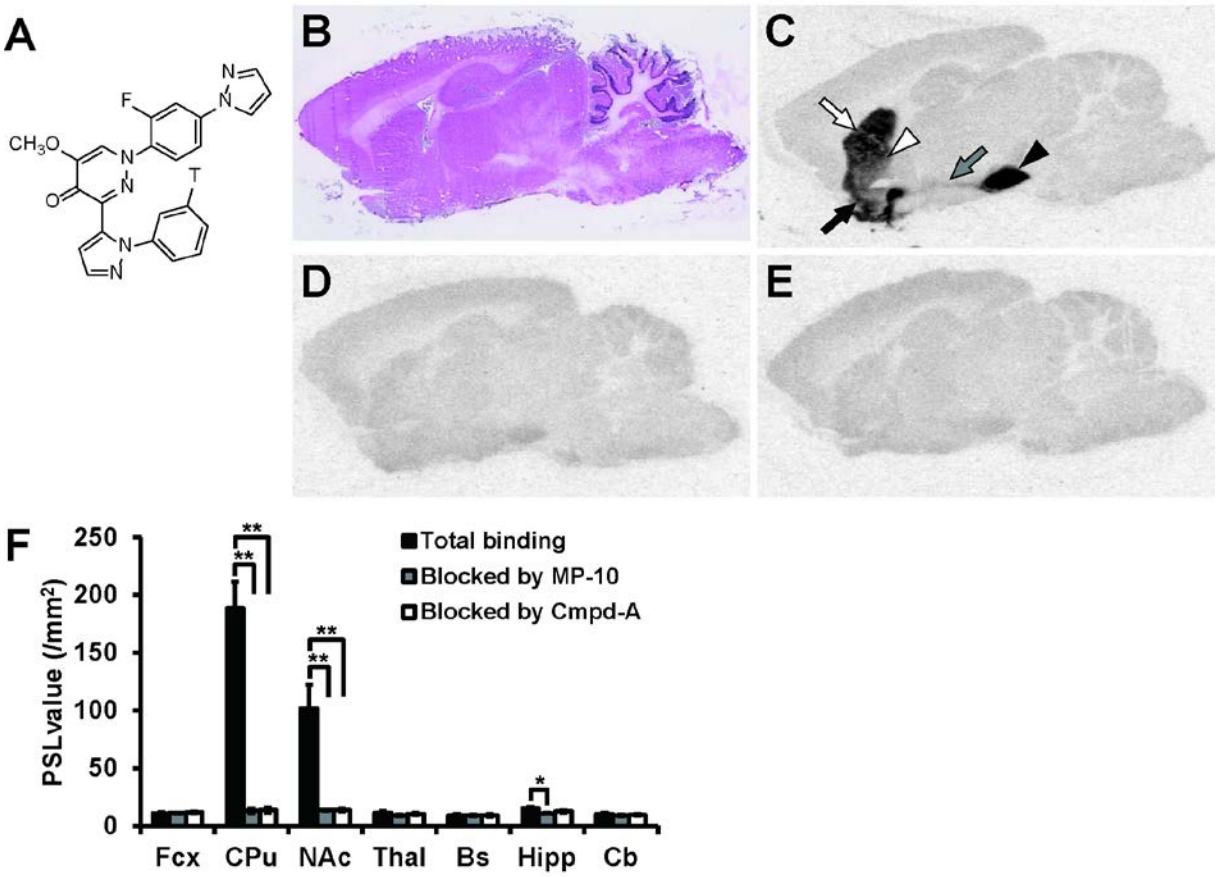

Figure 2. ***In vitro*** **autoradiography (ARG) using [^{3}H]Cmpd-A in sagittal rat brain sections.** The chemical structure of [^{3}H]Cmpd-A (A). Sections adjacent to those used for *in vitro* ARG of [^{3}H]Cmpd-A, were stained with hematoxylin and eosin (B). The autoradiogram shows the high accumulation of [^{3}H]Cmpd-A in the caudate putamen (CPu; white arrow), nucleus accumbens (NAc; black arrow), globus pallidus (GP; white arrow head), substantia nigra (SN; black arrow head), and striatonigral projection (gray arrow; C). *In vitro* ARGs in the presence of an excess amount of MP-10 (D) or Cmpd-A (E) were performed with adjacent sections. Radioactivity levels in several brain regions were represented as photostimulated luminescence (PSL) values in the presence or absence of an excess amount of MP-10 or Cmpd-A (F). Statistical analyses were performed using Dunnett's test (*$P \leq 0.05$, **$P \leq 0.01$

vs total binding, n=3). Fcx, frontal cortex; Thal, thalamus; Bs, brainstem; Hipp, hippocampus; Cb, cerebellum.

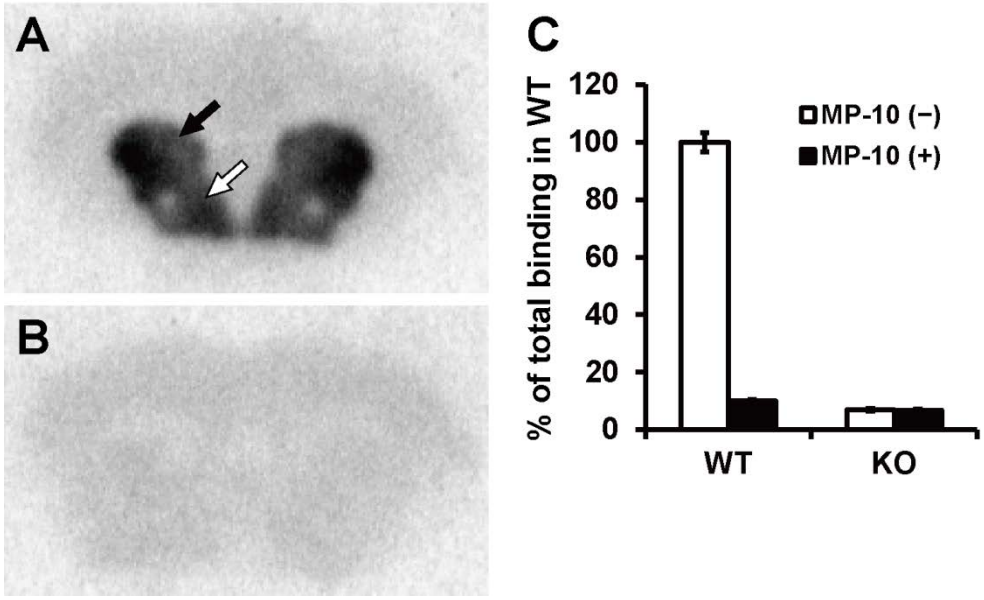

Figure 3. *In vitro* autoradiography (ARG) using [^{3}H]Cmpd-A in mouse brain sections. [^{3}H]Cmpd-A selectively accumulated in the caudate putamen (CPu; black arrow) and nucleus accumbens (NAc; white arrow) of wild-type (WT) mouse brain sections (A). The selective accumulation of [^{3}H]Cmpd-A in these areas did not occur in *Pde10a*-KO mouse brain sections (B). Radioactivity levels in the CPu of brain sections in the presence and absence of an excess amount of MP-10 are represented as a percent of total binding of WT mice (C). Data are represented as mean ± SEM.

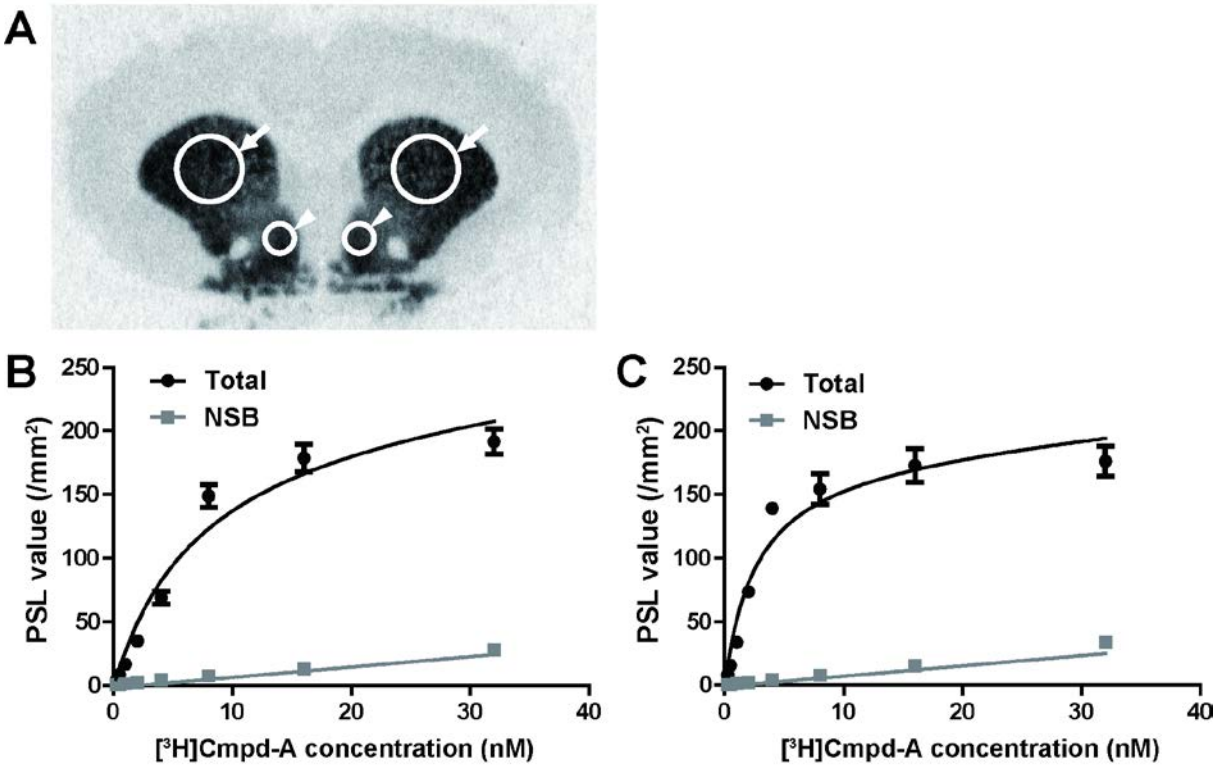

Figure 4. Saturation binding analysis using [^{3}H]Cmpd-A in rat brain coronal sections. A saturation binding assay was performed with a range of concentrations of [^{3}H]Cmpd-A. Regions of interest (ROIs) were the bilateral caudate putamen (CPu; arrows) and nucleus accumbens (NAc) shell (arrowheads) in the autoradiograms (A). Total and non-specific binding in each ROI was represented as PSL values (/mm^2), and saturation binding curves from the CPu (B) and NAc shell (C) were analyzed by nonlinear regression. K_d values in the CPu and NAc shell were estimated at 7.2 ± 1.2 nM and 2.6 ± 0.5 nM, respectively. All data were represented as mean ± SEM.

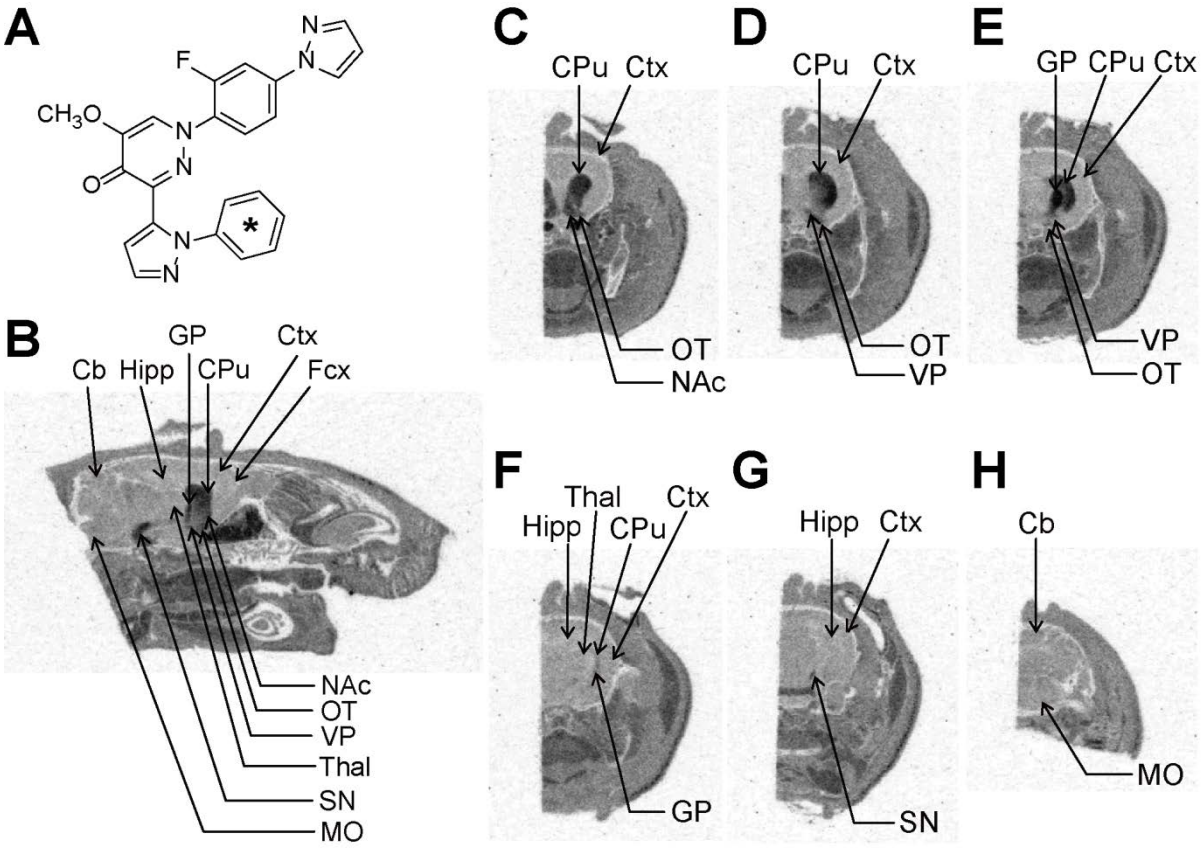

Figure 5. ***In vivo*** **ARG of [^{14}C]Cmpd-A in rats.** The chemical structure of [^{14}C]Cmpd-A (A). The asterisk denotes the labeled position. Autoradiograms of head sections were obtained from male rats 6 h after single oral administration of [^{14}C]Cmpd-A. The autoradiograms of 40 µm sagittal sections between 2.1 to 2.4 mm lateral to midline were taken (B). The locations for each coronal section relative to the bregma were 1.7 to 1.2 mm (C), 0.48 to −0.26 mm (D), −0.4 to −0.8 mm (E), −2.8 to −3.1 mm (F), −6.0 to −6.3 mm (G), and −12.7 to −12.8 mm (H). Acc, nucleus accumbens; Cb, cerebellum; Cpu, caudate putamen; Ctx, cortex; Fcx, frontal cortex; GP, globus pallidus; Hipp, hippocampus; MO, medulla oblongata; OT, olfactory tubercle; SN, substantia nigra; Thal, thalamus; VP, ventral pallidum.

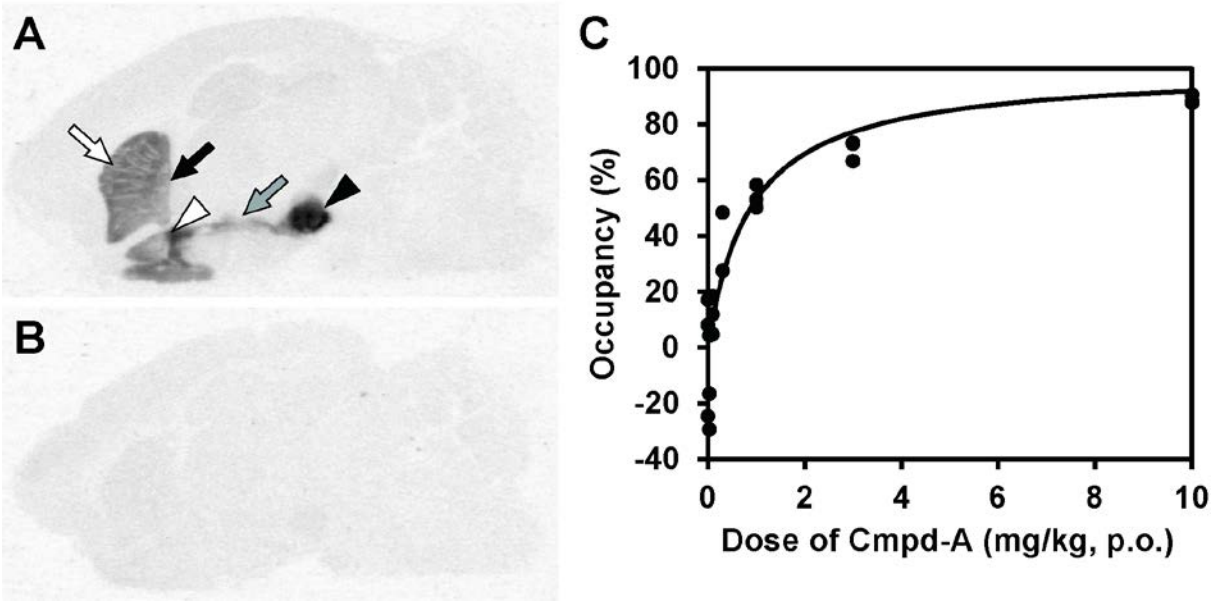

Figure 6. *In vivo* occupancy study of Cmpd-A using T-773 as a tracer in rats. In *in vitro* ARG study using the rat brain sagittal section, [^{3}H]T-773 selectively accumulated in the caudate putamen (CPu; white arrow), globus pallidus (GP; black arrow), nucleus accumbens (NAc; white arrow head), substantia nigra (SN; black arrow head), and striatonigral projection (gray arrow), where PDE10A is highly expressed (A). This accumulation was almost completely blocked by an excess amount of Cmpd-A (B). PDE10A occupancy (%) in the striatum was plotted against doses of orally administered Cmpd-A in rats with intravenous T-773 injection (C). The cerebellum was used as a reference region. PDE10A occupancy was increased in a dose-dependent manner. Oral administration of 0.88 mg/kg of Cmpd-A resulted in 50% PDE10A occupancy as determined by regression analysis.

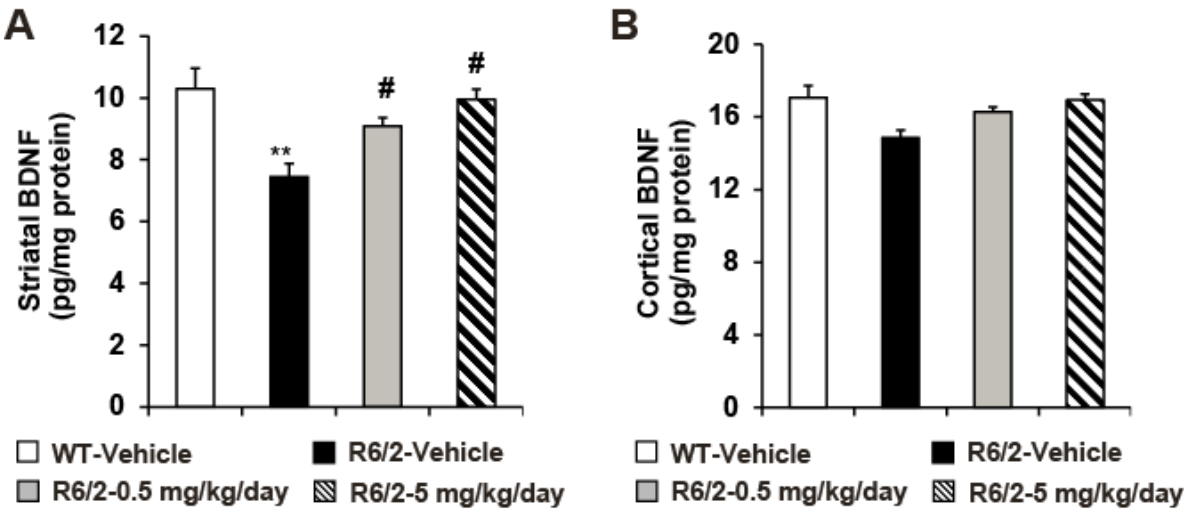

Figure 7. Effects of Cmpd-A on brain-derived neurotrophic factor (BDNF) levels in R6/2 mouse brain. BDNF protein levels in the striatum (A) and the cortex (B) of wild-type (WT) and R6/2 mice were measured by enzyme-linked immuno-sorbent assay at 12 weeks of age. Data are shown as mean + S.E.M. (n = 6 in each group). Statistical significance between WT and R6/2 mice was determined using Aspin–Welch test (**$P \leq 0.01$; versus vehicle-treated WT mice). Dose-dependent effects were statistically analyzed using two-tailed Williams' test (#$P \leq 0.05$; versus vehicle-treated R6/2 mice).

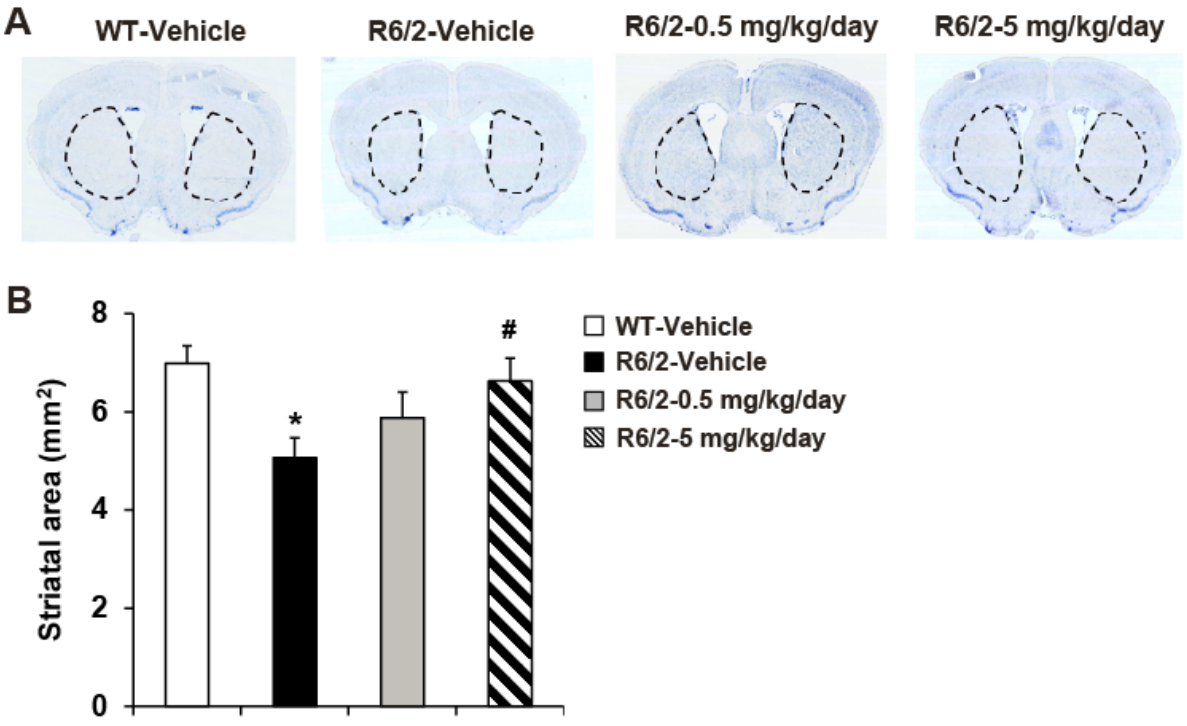

Figure 8. Effects of Cmpd-A on striatal atrophy in R6/2 mice. (A) Representative Nissl-stained coronal sections from mouse brains prepared at 12 weeks of age are shown. The dotted lines outline the striatum. (B) Striatal areas (mm^2) in the sections were measured to evaluate striatal atrophy. Data are represented as mean + S.E.M. (n = 4 in each group). Statistical significance between wild-type (WT) and R6/2 mice was determined using Aspin–Welch test (*$P \leq 0.05$; versus vehicle-treated WT mice). Dose-dependent effects were statistically analyzed using two-tailed Williams' test (#$P \leq 0.05$; versus vehicle-treated R6/2 mice).

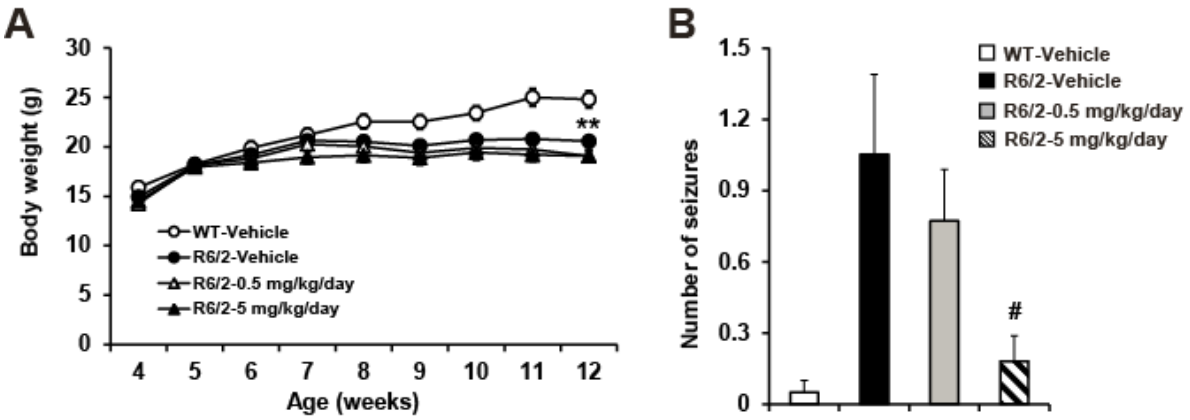

Figure 9. Effects of Cmpd-A on body weight changes and seizure frequency in R6/2 mice.

(A) Mice were weighed once per week throughout the study. Data are represented as mean ± S.E.M. [n = 20 in vehicle-treated wild-type (WT) mice, n =19 vehicle-treated R6/2 mice, n = 22 in Cmpd-A-treated R6/2 mice]. At 12 weeks of age, the body weight of vehicle-treated R6/2 mice was significantly lower than that of vehicle-treated WT mice (**$P \leq 0.01$). Daily treatment with Cmpd-A at 0.5 and 5 mg/kg/day for 8 weeks did not significantly prevent the suppression of body weight gain in R6/2 mice. Statistical significance between WT and R6/2 mice at 12 weeks of age was determined using Aspin–Welch test (**$P \leq 0.01$; versus vehicle-treated WT mice), and dose-dependent effects were statistically analyzed using two-tailed Williams' test (versus vehicle-treated R6/2 mice). (B) The number of seizures observed during the first 3 days of the acquisition phase in the procedural water T-maze test. All data are indicated as mean + S.E.M. (n = 20 in vehicle-treated WT mice, n =19 in vehicle-treated R6/2 mice, n = 22 in Cmpd-A-treated R6/2 mice). Dose-dependent effects were statistically analyzed using two-tailed Shirley–Williams test (#$P \leq 0.05$; versus vehicle-treated R6/2 mice).

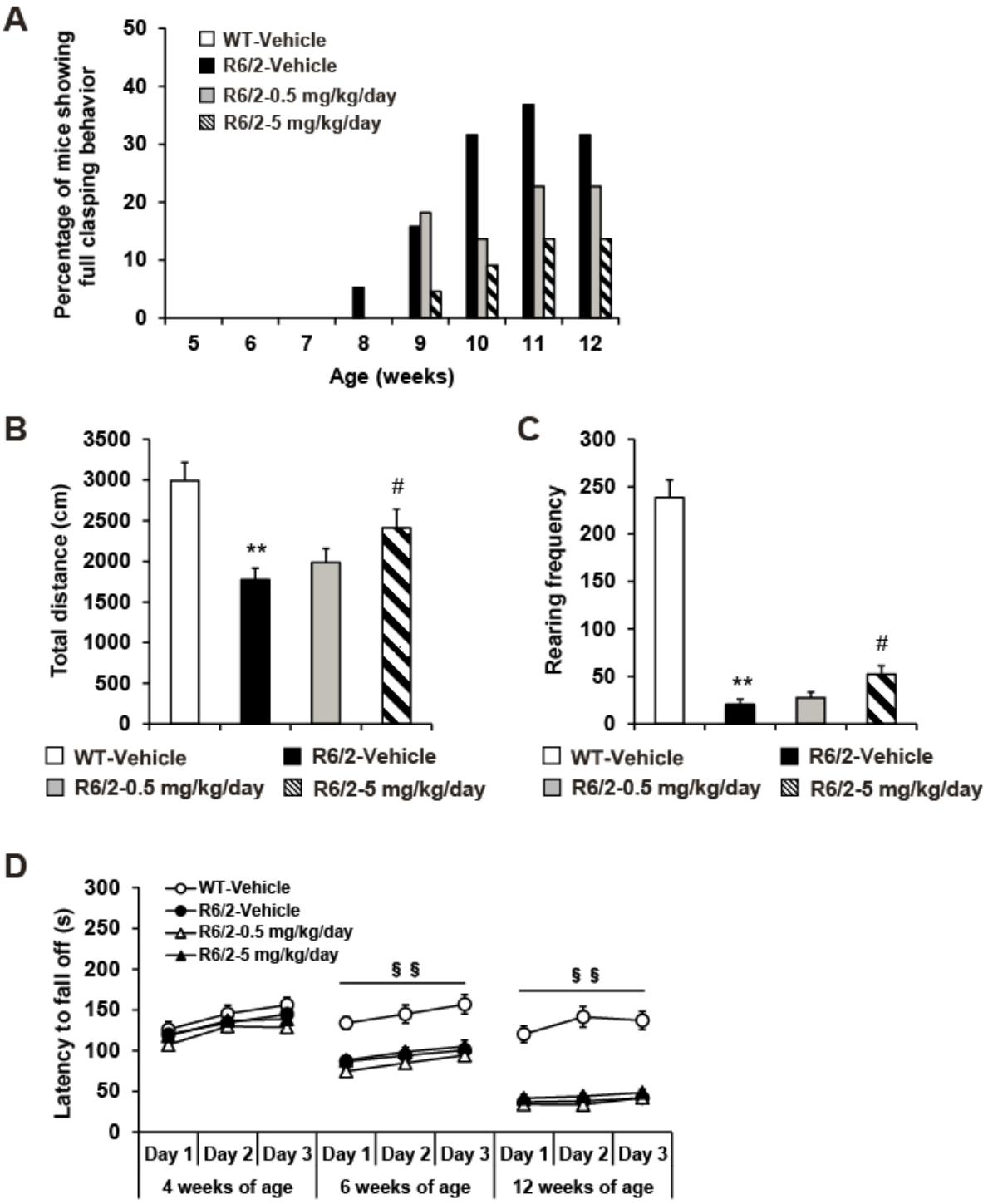

Figure 10. Effects of Cmpd-A on motor deficits in R6/2 mice. (A) Clasping behavior was evaluated once per week at 5–12 weeks of age. Data are represented as the percentages of mice showing full clasping behavior within 30 s of tail suspension [n = 20 in vehicle-treated wild-type (WT) mice, n =19 in vehicle-treated R6/2 mice, n = 22 in Cmpd-A–treated R6/2

mice]. (B and C) An open field test was performed at 12 weeks of age. Locomotor activities of mice were measured by two distinct indicators, total distance traveled (B) and rearing frequency (C). Data are represented as mean + S.E.M. (n = 20 in vehicle-treated WT mice, n =19 in vehicle-treated R6/2 mice, n = 22 in Cmpd-A-treated R6/2 mice). Statistical significance between WT and R6/2 mice was determined using Aspin–Welch test (**$P \leq 0.01$; versus vehicle-treated WT mice), and dose-dependent effects were statistically analyzed using two-tailed Shirley–Williams test (#$P \leq 0.05$; versus vehicle-treated R6/2 mice). (D) Motor coordination was assessed as the latency to fall off from a rotarod at 4, 6, and 12 weeks of age. Data are represented as mean ± S.E.M. (n = 20 in vehicle-treated WT mice, n =19 in vehicle-treated R6/2 mice, n = 22 in Cmpd-A–treated R6/2 mice). Differences between WT and vehicle-treated R6/2 mice at each week of age were analyzed using a repeated measures analysis of variance (RM-ANOVA). The RM-ANOVA showed a significant effect of test day at 4 weeks of age, significant effects of genotype and test day at 6 weeks of age, and significant effects of genotype and test day, and a significant genotype × test day interaction at 12 weeks of age. §§$P \leq 0.01$, a significant effect of genotype.

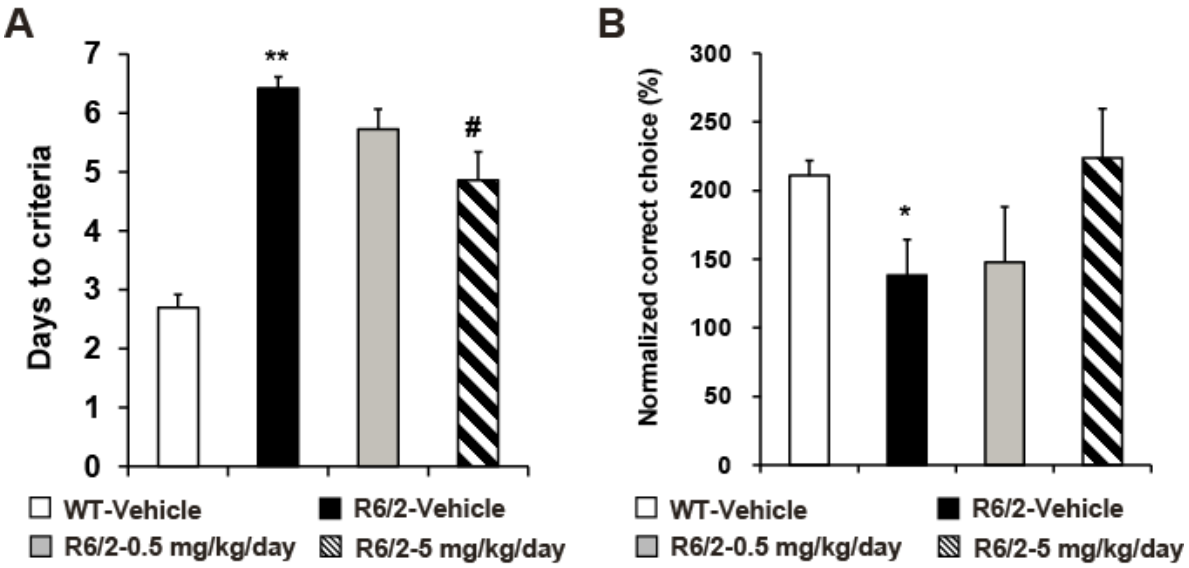

Figure. 11. Effects of Cmpd-A on impairment of procedural learning and cognitive flexibility in a procedural water T-maze task in R6/2 mice at 9–10 weeks of age. (A) The number of days to reach criteria during the acquisition phase is shown. Repeated treatment with Cmpd-A dose-dependently and significantly reduced the number of days required to meet the criteria in R6/2 mice. Data are indicated as mean + S.E.M. [n = 20 in vehicle-treated wild-type (WT) mice, n =19 in vehicle-treated R6/2 mice, n = 22 in Cmpd-A-treated R6/2 mice]. Statistical significance between WT and R6/2 mice was determined using Aspin–Welch test (**$P \leq 0.01$; versus vehicle-treated WT mice). Dose-dependent effects were statistically analyzed using two-tailed Williams' test (#$P \leq 0.05$; versus vehicle-treated R6/2 mice). (B) Once the criteria were achieved within 7 days in the acquisition phase, the animals progressed to the reversal phase on an individual basis. Effects of repeated treatment with Cmpd-A on reversal learning in R6/2 mice were evaluated. Data are expressed as the percentage of correct choices during days 4 to 6, normalized by the percent correct on Day 1,

and are presented as mean + S.E.M. (n = 20 in vehicle-treated WT mice, n = 8 in vehicle-treated R6/2 mice, n = 11 in Cmpd-A–treated R6/2 mice). Statistical significance between WT and R6/2 mice was determined using Aspin–Welch (*$P \leq 0.05$; versus vehicle-treated WT mice).

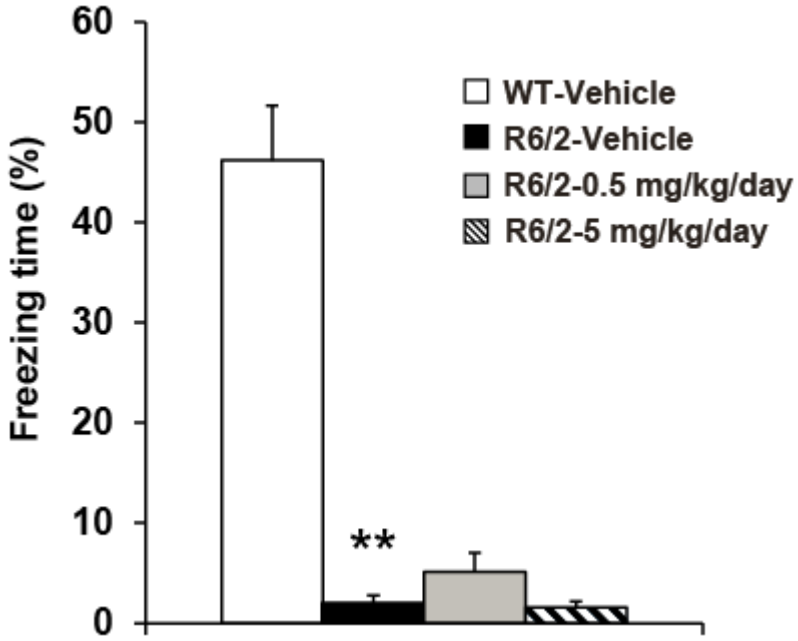

Figure 12. Effects of Cmpd-A on memory deficits in a contextual fear conditioning (CFC) test in R6/2 mice at 11 weeks of age. Data are represented as percent freezing time relative to total measuring time (180 s), and indicated as mean + S.E.M. (n = 20 in vehicle-treated WT mice, n =19 in vehicle-treated R6/2 mice, n = 22 in Cmpd-A-treated R6/2 mice). Statistical significance between WT and R6/2 mice was determined using Aspin–Welch test (**$P \leq 0.01$; versus vehicle-treated WT mice).